JOURNAL OF GEOPHYSICAL RESEARCH, VOL. 90, NO. B1, PAGES 685–701, JANUARY 10, 1985

Heat Flow in the Balearic and Tyrrhenian Basins, Western Mediterranean

I. HUTCHISON,[1,2] R. P. VON HERZEN,[3] K. E. LOUDEN,[4]
J. G. SCLATER,[5] AND J. JEMSEK[6]

We present the results of three detailed heat flow surveys which are used to investigate the variations of heat flow and age of the Balearic and Tyrrhenian basins in the western Mediterranean. Analysis of 12 measurements within a 10-km radius from 40°01'N, 4°55'E in the Balearic abyssal plain shows a mean heat flow of 92 ± 10 mW m^{-2}. After correction for the effects of sedimentation this value agrees well with the predictions of plate cooling and high extension stretching models for crust of the late Oligocene age proposed for the basin. A similar survey with 18 measurements around 40°16'N, 11°19'E in the Western Tyrrhenian gives a flux of 134 ± 8 mW m^{-2}, while the third survey of 26 measurements in the southern Tyrrhenian abyssal plain at 37°17'N, 12°58'E yields a slightly higher heat flow of 151 ± 10 mW m^{-2}. These values are within the range predicted by simple plate cooling models for the late Miocene ages of the deep Tyrrhenian basin. Thus our observations suggest that although the mode of crustal formation of these deep marginal basins is less well defined than that of the major ocean basins, the thermal signature is similar. Also, the trend of increasing heat flow from west to east through the Balearic and Tyrrhenian basins is in agreement with models of the formation of the western Mediterranean behind an eastwardly migrating trench system. In all three areas the measured flux shows significant local variability. In the two westernmost surveys this can be attributed to the presence of buried, high-conductivity salt structures, but in the third area (SE Tyrrhenian) the magnitude of the variations is several times greater than can be attributed to steady state thermal refraction alone. Instead, evidence exists for localized hydrothermal activity linked to the small topographical relief within the survey area.

INTRODUCTION

Three detailed heat flow surveys were completed on the RRS *Shackleton* cruise 3/81. The first consisted of 12 individual values within a 10-km radius survey area centered on 40°01'N, 4°55'E in the Balearic abyssal plain, with the second and third, of 18 and 26 values, respectively, around 40°16'N, 11°19'E and 39°17'N, 12°58'E in the Tyrrrhenian Sea (Figure 1). The survey sites were chosen to minimize any localized perturbation of the geothermal flux, either from refraction of heat through high-conductivity salt diapirs (Balearic) or by hydrothermal exchange through exposed basement outcrops and seamounts (Tyrrhenian). The first two areas have complete sedimentary cover and are several tens of kilometers from the nearest major topographic feature. Only D3 shows slight bathymetric relief across the study area and thinning of sediments (near outcrops?) over parts of the elevated basement structure.

The measurements have been used to form some of the first reliable estimates of area mean heat flows in the western Mediterranean. After correction for reductions due to sedimentation the values are combined with geological estimates of the basin ages to allow comparison of the heat flow with the predictions of the plate cooling and lithospheric stretching models. Despite the careful choice of sites, significant variability in the measured heat flow is found in all three surveys. Numerical modeling has shown that thermal refraction can account for the scatter in heat flow at sites D1 and D2, but hydrothermal or other processes are required to explain the larger anomalies found in area D3.

The average values from the three surveys can be used to estimate the variation of heat flow with age in young marginal basins. *Sclater et al.* [1980] and *Anderson* [1980] review marginal basin heat flows and find that values derived from "reliable" measurements (mostly from crust older than 20 Ma) show the same dependence on age as that found from the major ocean basins. Thus, while the specific nature of intrusion and crustal formation in marginal basins is not so clearly defined as for a mid-ocean spreading center, it appears that the thermal structure and properties of deep marginal sea and normal oceanic lithosphere are similar. This result supports the views of *Karig* [1970] and others that marginal basins are formed by extensional processes much like those occurring at active spreading centers. It should be noted, however, that while the heat flux–age relation holds well for marginal basins, their depths are typically 0.5–1.0 km greater than those of normal ocean crust of the same age [*Louden*, 1980].

The initiation and early stages of marginal basin formation are perhaps best understood in terms of simple lithospheric stretching models [e.g., *McKenzie*, 1978*a*]. Initially, the brittle continental crust and ductile lithosphere are stretched by an amount β. The isotherms are compressed as hot asthenosphere is brought closer to the surface, causing an increase in the heat flux. After extension the thermal transient gradually relaxes to the equilibrium value. If β is small, the crust is attenuated but maintains a finite thickness across the basin. If stretching continues, the original continental material forms a thinned and subsided margin, while oceanic crust is created in the central rift. Oceanic volcanism and crustal accretion represent the case of infinite stretching ($\beta = \infty$), and the central region of the basin then behaves as predicted by the oceanic plate model [e.g., *Parsons and Sclater*, 1977]. It is thought that processes similar to these have created the Oligocene and Miocene basins of the western Mediterranean, where both the Balearic and Tyrrhenian seas show aspects of dual oceanic and continental origins.

[1]Bullard Laboratories, Department of Earth Sciences, University of Cambridge, England.
[2]Now at B. P. Exploration, London, England.
[3]Woods Hole Oceanographic Institution, Massachusetts.
[4]Department of Oceanography, Dalhousie University, Halifax, Nova Scotia.
[5]Institute for Geophysics, University of Texas at Austin.
[6]Department of Earth, Atmospheric and Planetary Sciences, Massachusetts Institute of Technology, Cambridge.

Copyright 1985 by the American Geophysical Union.

Paper number 4B1182.
0148-0227/85/004B-1182$05.00

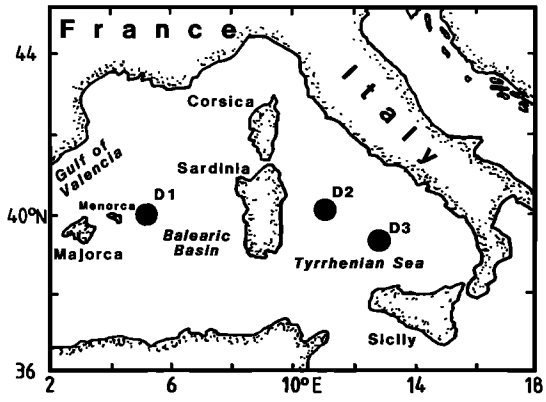

Fig. 1. Location of heat flow surveys, *Shackleton* 3/81.

The data presented in this paper have been compared with both plate and stretching models to distinguish between modes of basin formation. Reflecting younger crustal ages, the heat flow increases from west to east through the Balearic and Tyrrhenian basins. Only those models with large amounts of extension and ocean plate formation ($\beta = \infty$) predict values similar to the observed heat flows for the estimated basin ages. The measured values are in agreement with the trends found in older marginal basins elsewhere and do not differ significantly from the heat flux expected from normal ocean crust of the same age.

THE WESTERN MEDITERRANEAN

Recently, new geophysical data [*Finetti and Morelli*, 1973; *Hsu et al.*, 1978] and the advent of models of basin development and margin formation by continental stretching [*McKenzie*, 1978*a*, *b*] have greatly increased our understanding of the evolution of the western Mediterranean. *Biju-Duval et al.* [1978] and *Hsu* [1978] give comprehensive syntheses of the current knowledge of the tectonic development of the region; these, with additional data, have been used to form the following summary of the formation and history of the Balearic and Tyrrhenian basins.

The Balearic/Provencal Basin

During late Oligocene/early Miocene time the Sardinia and Corsica continental blocks moved away from the European plate by a combination of eastward translation and counterclockwise rotation [*Montigny et al.*, 1981; *Alvarez et al.*, 1974; *Auzende et al.*, 1973]. This movement opened the Balearic basin and created stretched passive margins in the Gulf of Lyons, on the Menorca rise and to the west of Sardinia and Corsica (Figure 2) [after *Biju-Duval et al.*, 1978]. While the precise mechanism of opening is poorly known, the basin may have formed in a back arc setting behind an eastwardly migrating arc-trench system [*Alvarez et al.*, 1974; *Boccaletti and Guazzone*, 1974].

The timing of opening is inferred from the following geophysical and geological evidence:

1. Drilling at site 372 on the Menorca rise established that the basin was already deep in the lower Burdigalian, 19–22 Ma [*Hsu et al.*, 1978].

2. Drilling in the Gulf de Lyons encountered shallow marine sediments of Aquitanian age, 22–24 Ma; seismic reflection data show that only the lowest layers of these are affected by the faulting which formed the margin, suggesting that rifting ceased in the Aquitanian.

3. Paleomagnetic and K-Ar data from the Tertiary volcanic rocks of Sardinia suggest that the block underwent a rotation of approximately 30° between 22 and 19 Ma [*Montigny et al.*, 1981].

4. The Balearic was probably formed in the same extensional event that created the Gulf of Valencia between Menorca and Northern Spain. This opening has been dated at 21 ± 2 Ma from volcanic tuffs recovered in Deep Sea Drilling Project (DSDP) site 123 in the Valencia trough.

5. Geological evidence from southern France shows that a major transgression occurred in the Aquitanian (22–24 Ma) at which time the drainage pattern reversed from the northerly and westerly directions of Oligocene times to those observed today.

6. The andesitic volcanics of Oligocene and Miocene ages found in western Sardinia are similar to western Pacific island arc sequences and may mark the remnants of back arc volcanism created during the opening of the Balearic.

From the above data the best estimate of the age of formation of the Balearic basin has been assigned as 20–25 Ma.

The crustal structure of the Basin has been investigated using seismic refraction techniques [*Fahlquist and Hersey*, 1969; *Hinz*, 1972; *Finetti and Morelli*, 1973], showing 5–6 km

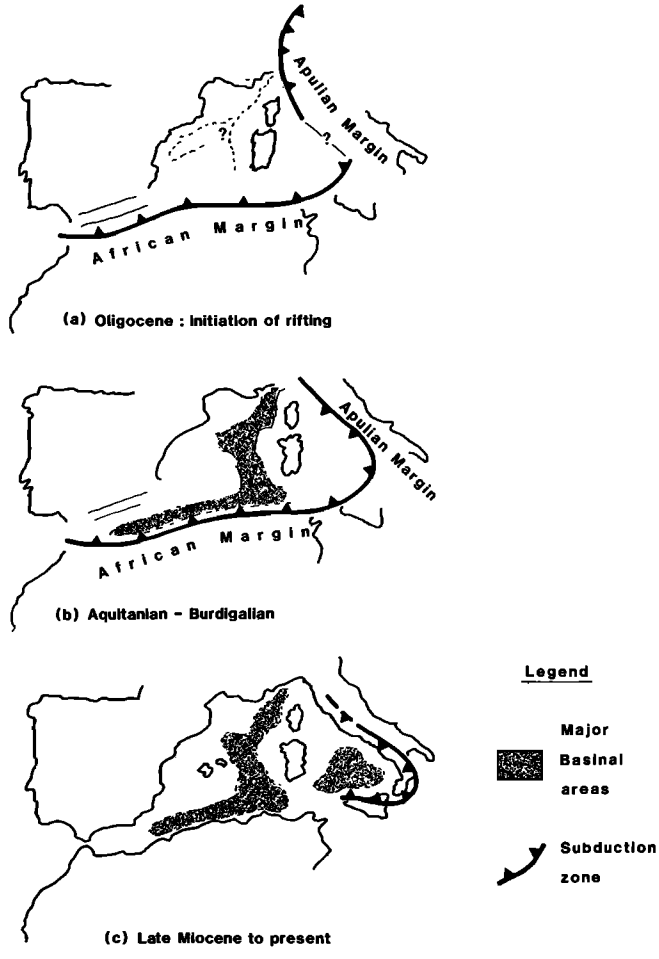

Fig. 2. Speculative evolution of the western Mediterranean since the Oligocene [after *Biju-Duval et al.*, 1978]; see text for discussion.

of sedimentary and evaporitic deposits over a thin (approximately 5 km) crust. Although no well-lineated anomalies can be clearly identified [*Galdeano and Rossignol*, 1977], an overall kinematic interpretation and structural (seismic) evidence suggest continental margin rifting separated by oceanic crust [*Burrus*, 1984]. Thus seismic and magnetic evidence both suggest that the crustal structure is oceanic. Seismic reflection profiles from the Balearic are dominated by strong reflections marking thick (<1 km) sequences of Messinian (6.6–5.2 Ma) salts and evaporites [*Montadert et al.*, 1978]. Through most of the abyssal plain intense halokinesis has occurred, forming diapiric structures which commonly penetrate the later sediments.

The Tyrrhenian Sea

It is generally believed that the Tyrrhenian Sea formed by mid-late Miocene extension behind a southeastwardly migrating trench-arc system (Figure 2). The western limit of the basin is characterized by the tilted fault blocks of the passive margin with Sardinia, while the southeast extreme is bounded by Sicily, Calabria, and the Eolian Islands. These latter features probably mark an island arc system associated with the subduction of Mesozoic crust of the Ionian sea, as is suggested by a WNW dipping Benioff zone extending from Calabria beneath the Tyrrhenian Sea [*Ritsema*, 1970; *Lort*, 1978] and the contemporaneaous existence of calc-alkaline arc-type volcanism in the Eolian Islands and basaltic oceanic volcanism in the abyssal plain [*Barberi et al.*, 1973].

Seismic reflection and refraction analysis from the central Tyrrhenian area shows a thin crust beneath the surficial sediments [*Finetti and Morelli*, 1973; *Nicholich*, 1981; *Duschenes*, 1983]. Firm evidence of the age and oceanic nature of the basin was obtained from drilling at DSDP site 373 which recovered 3–8 Ma basalts from the edge of a small seamount in the central abyssal plain [*Barberi et al.*, 1978]. The geochemical signature of these lavas shows no evidence of contamination by continental crust.

Extensive seismic reflection coverage reveals a much thinner sedimentary sequence than that encountered in the Balearic basin. The thickness and extent of pre-Messinian sediments are poorly known but are probably limited to a few hundred meters. Messinian salt and evaporite are evident throughout much of the basin, although the continuity and volume of the deposits are limited in the south and east. Thick (>1 km) deposits are only well developed in the Cornaglia basin at the base of the Sardinia rise, and even here, widespread diapirism is absent. The occurrence of Messianian evaporites and erosional surfaces [*Ryan and Cita*, 1978; *Fabbri and Curzi*, 1979; *Malinverno et al.*, 1981] indicates that the Tyrrhenian formed an extensive deep basin at the end of the Miocene. Further, since salt is expected to form first in the deepest areas [*Hsu et al.*, 1973], the detailed distribution of the Messinian deposits suggests that the basin was shallower in the southeast at that time. Consequently, the southeastern abyssal plain may have undergone considerable post-Messinian subsidence to attain its present depth [*Fabbri and Curzi*, 1979].

From this evidence it appears that the Tyrrhenian basin predates the Messinian by only a few million years in the west and may be of a similar age in the southeast. This conclusion agrees with the age limits set by the dates of the site 373 basalts and the general lack of thick pre-Messinian sediment sequences. Thus the best estimates of the age of the Tyrrhenian basin have been taken as approximately 7–12 Ma in the west (area D2) and 5–8 Ma in the southeast (area D3).

INSTRUMENTATION AND TECHNIQUES

Heat Flow

Two separate groups operated heat flow systems on the *Shackleton* cruise 3/81; 36 values were obtained using a violin-bow instrument recently developed in Cambridge [*Hutchison*, 1983], while the remaining measurements were taken using the Woods Hole Oceanographic Institution (WHOI) digital heat flow system. The Cambridge instrument was fitted with a 7.9-mm-diameter sensor tube containing nine individual thermistors over a 4-m spacing and included heating elements to allow in situ measurement of thermal conductivity using a heat pulse technique [e.g., *Lister*, 1979; *Hyndman et al.*, 1979]. Owing to an instrumental malfunction, no in situ conductivities were recorded on the first deployment (survey D1), but all subsequent stations using the Cambridge probe included extensive in situ values. Both instruments recorded the temperature data on digital cassette tape with a resolution of 0.5 mK and simultaneously telemetered information to the ship for real-time monitoring. Unlike the Cambridge instrument, the WHOI gear consisted of conventional outrigger probes fixed to a long strength member. The WHOI probes were fitted with a secondary heating element through which a constant heating current could be passed to allow in situ measurement of thermal conductivity. In practice, useful conductivity values were returned with this prototype system only on the last few stations of the cruise. Although the WHOI instrument recorded fewer temperature points than the Cambridge instrument, the resultant temperature profiles had the advantage of a slightly greater penetration (5.5 compared with 4.0 m). Both instruments were used in a "pogo" fashion, allowing multiple penetrations to be made on a single lowering. The measured temperature profiles (shown in Appendix A[1]) were generally linear, with no significant evidence of large-scale systematic curvature found at any of the three survey sites.

A piston core was taken in each area to allow on-board analysis of the sediment thermal conductivity by needle probe techniques [*Von Herzen and Maxwell*, 1959]. Both groups took independent sets of measurements, WHOI using an automatic multiple needle instrument and Cambridge using a simpler, analogue recording probe. This allowed cross calibration of the two instruments, and, in general, the values obtained agreed to within 10%. Conductivities measured on the core samples (after correction for ambient pressure and temperature at the seafloor [*Ratcliffe*, 1960]) showed close correlation with the in situ values obtained at surrounding stations (Figure 3). The in situ values are consistently a few percent higher than the core values (although still within the experimental errors); this may be a result of the introduction of excess water into the cores by suck-in and physical disturbance of the sediment fabric caused by the coring process. Core positions and mean conductivities are given in Table 1 and the individual values plotted in Figure A1, Appendix A.

Navigation

The ship's navigation used both Loran C and satellite. While the Loran values were internally more consistant, they were normally displaced by a uniform amount from the posi-

[1]Appendix A is available with entire article on microfiche. Order from American Geophysical Union, 2000 Florida Avenue, N.W., Washington, D. C. 20009. Document 4B-013; $2.50. Payment must accompany order.

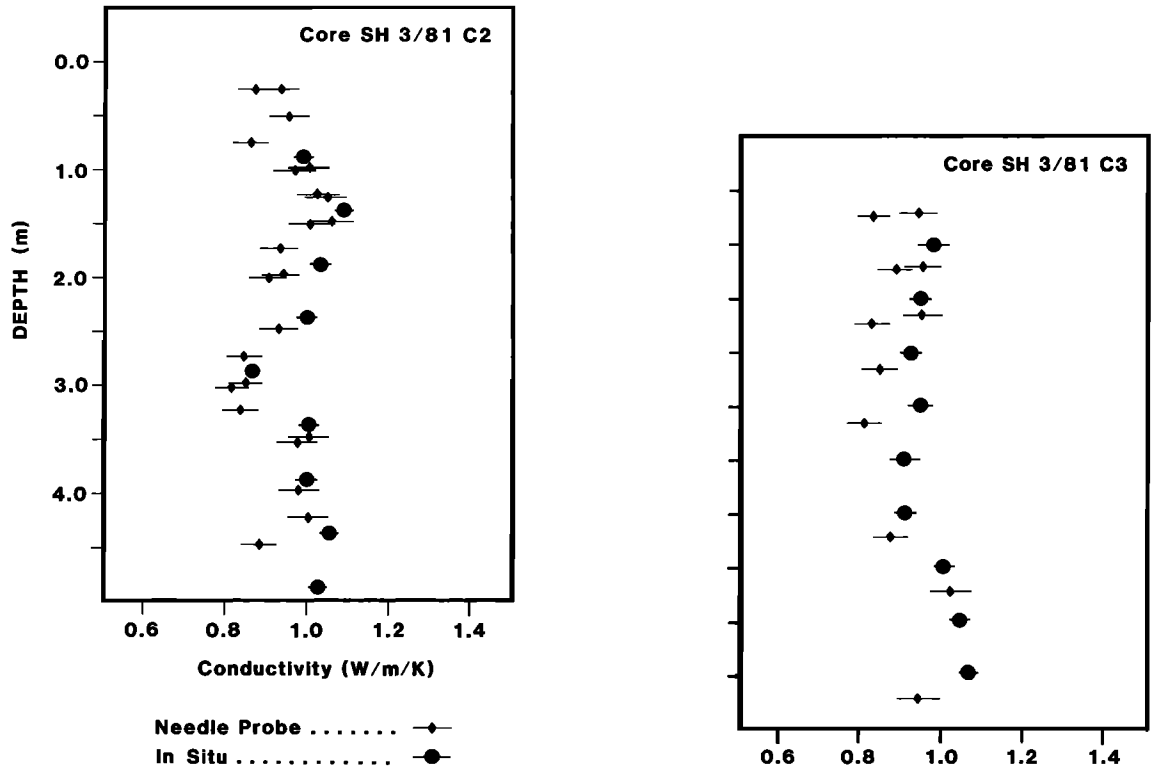

Fig. 3. Comparison of in situ and core needle probe conductivity measurements at sites D2 and D3 in the Tyrrhenian Sea.

tion computed by satellite and dead reckoning. Since satellites give a better estimate of the absolute position, the Loran values have been migrated to coincide with the net of positions defined by the reliable satellite fixes. The offsets were usually less than 0.1–0.2 arc min and, although varying between survey areas, did not change appreciably during the course of a lowering. The combination of Loran and satellite navigation yields a positional accuracy of better than a few hundred meters. The position of the probe relative to the ship may also be offset by some distance; elsewhere, similar surveys have shown that surface ship and instrument positions, (the latter based on acoustic navigation) may differ by up to 500 m. However, numerical modeling of the Cambridge probe towed on the *Shackleton* trawl wire (A. Bowen, personal communication, 1982) suggested that the differences would be less than 250 m for the towing speeds used in the survey.

Seismic Reflection Profiling

Single-channel seismic profiles were recorded on an analogue frequency-modulated system. The sound source was a single 160 inch^3, 1800 psi air gun fired once every 12 s, producing a signal dominated by a 1/4-s-long wave train with a dominant frequency of about 15 Hz. The replayed sections in Figures 5, 8, and 10 have been high-pass filtered at 60 Hz to reduce the reverberations and give a signal pulse of length less than 100 ms. In addition, linear time variable gain has been applied at a rate of 2 dB s^{-1}, starting 3.5 s after the air gun shot.

TABLE 1. Core Positions and Thermal Conductivities

Core	Latitude	Longitude	Length, m	$\bar{K}$, W m^{-1} K^{-1}
SH3/81C1	40°00.4'N	04°52.8'E	6.25	1.12 ± 0.06
SH3/81C2	40°14.5'N	11°17.6'E	8.25	0.94 ± 0.05
SH3/81C3	39°24.3'N	12°56.8'E	8.50	0.92 ± 0.08

$\bar{K}$ is the harmonic mean conductivity from needle probe measurements spaced at approximately 25-cm intervals along the core. Errors include a factor of 5% to account for the inaccuracy of the needle probe technique.

Data Reduction

Equilibrium sediment temperatures (referenced to the near-bottom water temperature) were estimated by extrapolating the recorded temperatures from the first few minutes after penetration using an $F(\alpha; t)$ function to describe the frictional heating transient [e.g., *Bullard*, 1954]. The small WHOI outrigger probes have a shorter time constant than the Cambridge sensor string, which allowed the simpler asymptotic form of $F(\alpha, t)$, i.e., $T \propto 1/t$, to be used for the WHOI data. Both instruments gave extrapolated temperatures with errors of a few millidegrees at worst. The sensor depths on the Cambridge probe are corrected for tilt using a continuous reading scalar tilt cell, so that their vertical separations are known within 1–2 mm; over the thermistor separations of 0.5–1.0 m this gives only negligible errors. The tilt of the WHOI instrument was monitored as either $0 < \theta < 15°$ or $15° < \theta < 30°$, thus introducing uncertainties of ~2 and ~5% in the sensor separations.

The temperature gradients G quoted are the least squares best fit lines through the equilibrium temperature depth profiles with the individual points weighted by the inverse square of their temperature errors. Following *Von Herzen et al.* [1982], the error ΔG in G has been calculated at the 95% confidence level. In situ conductivities were obtained for the Cambridge heat pulse probe using techniques similar to those

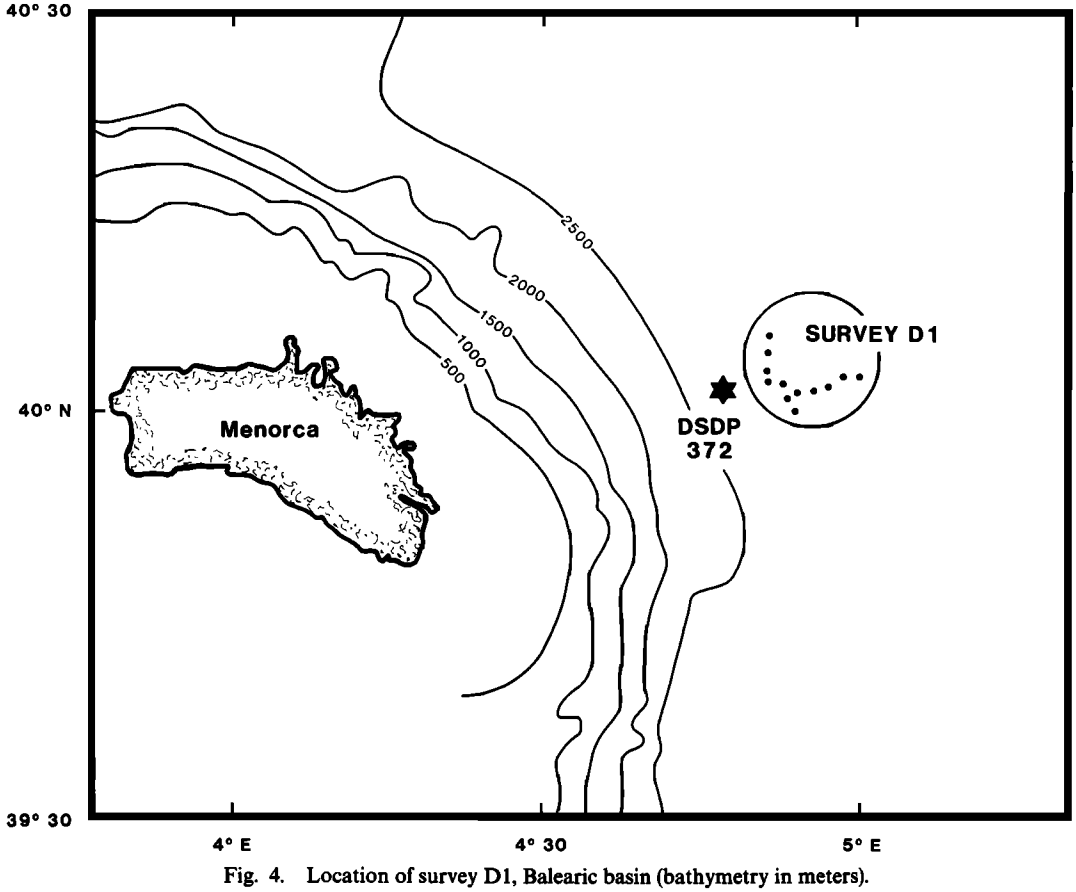

Fig. 4. Location of survey D1, Balearic basin (bathymetry in meters).

described by *Lister* [1979] and *Hyndman et al.* [1979]. For each individual measurement, care was taken to ensure that the extrapolated infinite time temperatures following the heat pulse agreed, to within the measurement accuracy, with the previously estimated equilibrium sediment temperatures. Satisfying this requirement implicitly accounts for the effects of the poorly conducting electrical insulation within the probe and any skin resistance between the probe and the sediments [*Hutchison*, 1983]. Data reduction for the continuous heating WHOI probes used an approximation to the cylindrical heating function $G(\alpha, t)$ to allow estimation of the sediment conductivities.

Where in situ values of conductivity K are available, the harmonic mean and 95% uncertainty (ΔK) have been calculated. At those stations where no in situ values were available, the survey mean estimate has been assigned. Because of uncertainties in the absolute values of conductivity determined either by needle probe [*Goldberg et al.*, 1980] or by the in situ heat pulse technique [*Hutchison*, 1983] further errors of 5 and 3% have been assigned to the core and in situ values, respectively.

The heat flux Q at each station has been calculated as

$$Q = GK$$

with the uncertainty:

$$\Delta Q = G\Delta K + K\Delta G$$

An alternative method of calculating Q for those stations with in situ values of conductivity was to multiply the temperature gradients between pairs of thermistors by the conductivity found at an intermediate sensor. This technique has the advantage of returning an improved estimate of the flux in areas where the conductivities vary strongly with depth, but in this case no significant differences resulted, either in Q or ΔQ.

For each survey the area weighted mean flux and a statistical estimate of its uncertainty were calculated as

$$\bar{Q} = \Sigma Q_i(W/\Sigma W_i) \qquad W_i = (\Delta Q_i/Q_i)^{-2}$$

and

$$\Delta Q = \sigma t(N-1)^{-1/2}$$

where σ is the standard deviation of the N values, Q_i and t are the Student's t parameter for $N-2$ degrees of freedom at the 97.5% confidence level (one sided).

SURVEY D1

Survey D1 consists of 12 individual measurements within a 10-km-radius survey area in the westernmost part of the Balearic abyssal plain (Figure 4). This particular site was chosen to avoid the major domes and ridges of Messinian salt encountered throughout much of the basin and to benefit from the control of the upper sedimentary structures and the heat flow measured at DSDP site 372, 10 km to the west.

The station positions and measured temperature profiles are plotted in Figures A2 and A3, and the results and listed in Table 2. Sections of the reflection profile SH3/81P1 are reproduced in Figure 5*a*, and the values and locations of the heat flow measurements are marked. The profile shows a sediment-filled depression, bounded to the north, west, and south by

TABLE 2a. RRS *Shackleton* 3/81 Heat Flow Data: Surveys D1 and D2

Station	Latitude N	Longitude E	Water Depth, m	N	Gradient, mK m^{-1}	K, W m^{-1} K^{-1}	Q, mW m^{-2}
D1 1.1	40°02.9′	05°00.7′	2713	5	87 ± 3	(1.12 ± 0.05)*	97 ± 7
1.2	40°03.6′	04°58.8′	2703	5	71 ± 3	(1.12 ± 0.05)*	79 ± 6
1.3	40°02.6′	04°57.7′	2699	5	70 ± 2	(1.12 ± 0.05)*	79 ± 6
1.4	40°02.5′	04°56.1′	2698	5	76 ± 28	(1.12 ± 0.05)*	85 ± 34
1.5	40°02.6′	04°54.9′	2698	5	73 ± 7	(1.12 ± 0.05)*	82 ± 11
D1 2.1	40°00.4′	04°54.0′	2701	6	74 ± 7	(1.15 ± 0.07)†	86 ± 15
2.2	40°01.6′	04°53.6′	2705	6	70 ± 9	(1.15 ± 0.07)†	82 ± 16
2.3	40°02.4′	04°52.9′	2709	5	71 ± 13	(1.15 ± 0.07)†	82 ± 19
2.4	40°02.8′	04°52.1′	2713	5	96 ± 13	(1.15 ± 0.07)†	110 ± 17
2.5	40°03.8′	04°51.5′	2717	5	101 ± 11	(1.15 ± 0.07)†	116 ± 16
2.6	40°04.6′	04°51.4′	2717	5	102 ± 11	(1.15 ± 0.07)†	117 ± 16
2.7	40°05.8′	04°51.8′	2721	5	85 ± 9	(1.15 ± 0.07)†	98 ± 13
D2 3.1	40°18.1′	11°20.5′	2862	6	128 ± 6	(1.01 ± 0.06)‡	129 ± 13
3.2	40°16.9′	11°19.7′	2834	6	114 ± 9	(1.01 ± 0.06)‡	115 ± 15
3.3	40°15.4′	11°19.0′	2866	6	145 ± 5	(1.01 ± 0.06)‡	146 ± 13
3.4	40°14.5′	11°18.2′	2878	6	115 ± 4	(1.01 ± 0.06)‡	116 ± 11
D2 4.1	40°13.6′	11°16.4′	2885	6	134 ± 4	(1.01 ± 0.06)‡	135 ± 12
4.2	40°12.1′	11°16.9′	2887	6	135 ± 4	(1.01 ± 0.06)‡	136 ± 12
4.3	40°10.3′	11°16.1′	2883	6	162 ± 5	(1.01 ± 0.06)‡	164 ± 15
4.4	40°09.4′	11°15.3′	2883	6	138 ± 12	(1.01 ± 0.06)‡	139 ± 20
4.5	40°08.2′	11°14.3′	2888	6	122 ± 11	(1.01 ± 0.06)‡	123 ± 18
D2 5.1	40°11.0′	11°24.5′	2856	6	107 ± 6	(1.01 ± 0.06)‡	108 ± 12
5.2	40°11.2′	11°22.5′	2858	6	150 ± 8	(1.01 ± 0.06)‡	151 ± 17
D2 6.1	40°11.8′	11°20.1′	2877	9	112 ± 3	1.06 ± 0.04	118 ± 7
6.2	40°12.7′	11°19.1′	2873	9	132 ± 3	1.04 ± 0.04	137 ± 10
6.3	40°13.4′	11°17.8′	2873	9	126 ± 3	1.00 ± 0.05	125 ± 9
6.4	40°13.9′	11°14.9′	2873	9	129 ± 3	0.99 ± 0.04	127 ± 8
6.5	40°14.8′	11°13.3′	2875	9	133 ± 3	1.02 ± 0.04	136 ± 10
6.6	40°14.2′	11°11.5′	2864	9	153 ± 4	0.99 ± 0.05	150 ± 12
6.7	40°14.1′	11°10.9′	2860	9	151 ± 3	1.02 ± 0.05	154 ± 12

N is the number of temperature points used in assigning the temperature gradient; Q is the heat flux; K is the thermal conductivity. Stations 1, 3, 5, 6: Cambridge violin bow heat flow instrument; Stations 2, 4: Woods Hole Oceanographic Institution outrigger heat flow probe.

*Harmonic mean K, core C1, upper 4 m.

†Harmonic mean K, core C1, upper 6 m.

‡Survey mean K from core C2 and station 6 in situ values.

TABLE 2b. *Shackleton* 3/81 Heat Flow Data: Survey D3

Station	Latitude N	Longitude E	Water Depth, m	N	Gradient, mK m^{-1}	K, W m^{-1} K^{-1}	Q, mW m^{-2}
D3 7.1	39°08.2′	12°57.5′	3445	9	143 ± 3	(0.95 ± 0.05)*	135 ± 10
7.2	39°09.2′	12°58.2′	3447	9	179 ± 8	0.93 ± 0.04	167 ± 16
7.3	39°10.3′	12°58.6′	3439	9	140 ± 4	0.96 ± 0.05	135 ± 11
7.4	39°12.5′	12°59.2′	3459	9	148 ± 3	0.92 ± 0.04	135 ± 8
7.5	39°13.6′	12°58.8′	3447	9	161 ± 5	0.95 ± 0.05	152 ± 12
7.6	39°14.8′	12°58.5′	3451	9	167 ± 5	0.93 ± 0.05	155 ± 12
7.7	39°15.9′	12°58.0′	3412	9	229 ± 5	0.96 ± 0.06	220 ± 17
D3 8.1	39°27.5′	12°56.7′	3577	9	146 ± 2	0.98 ± 0.05	143 ± 16
8.2	39°26.2′	12°56.8′	3574	9	144 ± 6	0.96 ± 0.04	137 ± 14
8.3	39°24.6′	12°56.9′	3569	9	154 ± 4	0.97 ± 0.04	150 ± 10
8.4	39°23.4′	12°57.0′	3558	9	93 ± 7	1.00 ± 0.05	93 ± 12
8.5	39°22.1′	12°57.1′	3506	5	147 ± 19	(0.96 ± 0.05)†	141 ± 25
8.6	39°21.1′	12°57.7′	3424	9	174 ± 13	0.94 ± 0.04	164 ± 19
8.7	39°20.1′	12°57.8′	3447	9	138 ± 4	0.94 ± 0.05	130 ± 10
8.8	39°19.0′	12°57.7′	3426	9	145 ± 4	0.96 ± 0.05	139 ± 11
D3 9.1	39°14.4′	13°09.5′	3569	6	145 ± 18	(0.97 ± 0.05)‡	141 ± 23
9.2	39°15.3′	13°07.5′	3570	6	155 ± 12	0.99 ± 0.06	153 ± 19
9.3	39°15.6′	13°06.1′	3566	5	168 ± 14	0.97 ± 0.06	163 ± 20
9.4	39°15.7′	13°04.7′	3526	5	164 ± 12	0.96 ± 0.06	157 ± 19
9.5	39°16.0′	13°03.4′	3487	5	142 ± 30	0.95 ± 0.06	135 ± 35
9.6	39°15.7′	13°01.8′	3507	6	171 ± 8	0.96 ± 0.06	164 ± 26
9.7	39°15.8′	13°00.6′	3487	5	160 ± 12	(0.97 ± 0.06)‡	155 ± 20
9.8	39°17.6′	12°58.8′	3319	6	218 ± 10	(0.97 ± 0.06)‡	211 ± 20
D3 10.1	39°16.4′	12°57.2′	3334	7	166 ± 10	0.96 ± 0.06	159 ± 20
10.2	39°16.7′	12°55.2′	3294	8	133 ± 11	(0.95 ± 0.06)*	126 ± 17
10.3	39°16.7′	12°53.2′	3367	8	137 ± 7	(0.95 ± 0.06)*	130 ± 14

N is the number of temperature points used in assigning the temperature gradient; Q is the heat flux; K is the thermal conductivity. Stations 7, 8, 10: Cambridge violin bow heat flow instrument; Station 9: Woods Hole Oceanographic Institution outrigger heat flow probe.

*Station 7 mean K (in situ).

†Station 8 mean K (in situ).

‡Station 9 mean K (in situ).

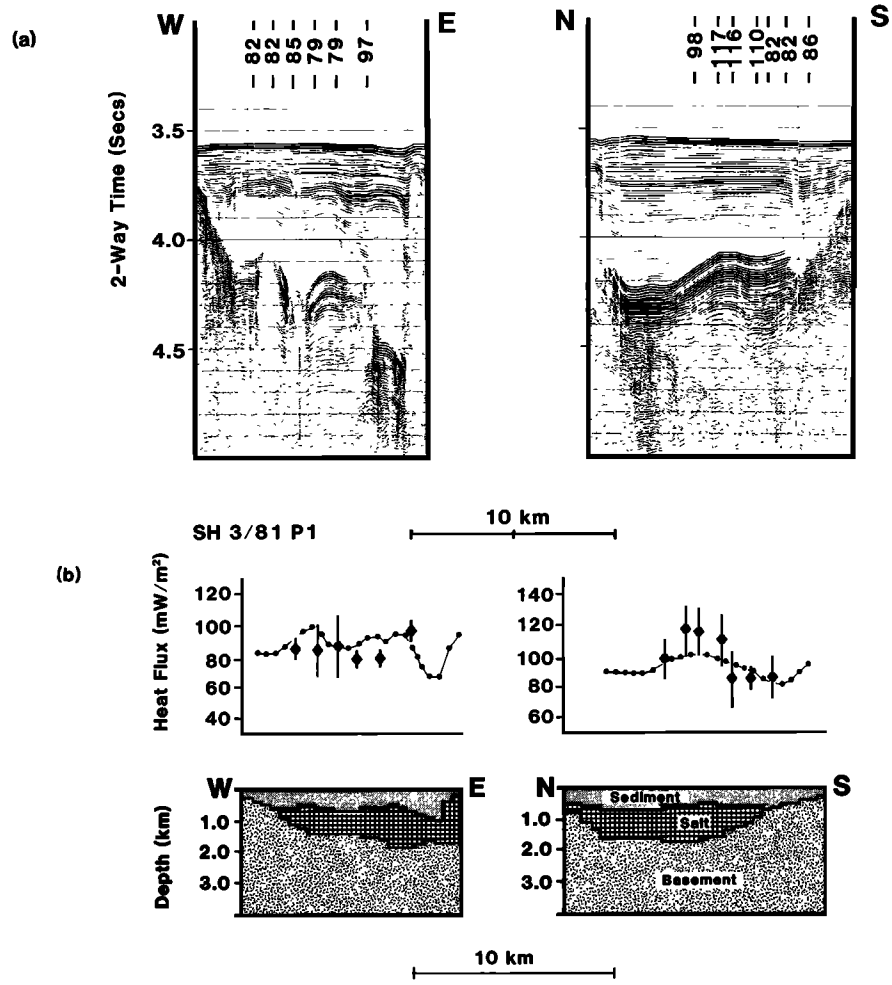

Fig. 5. (*a*) Reflection line SH3/81P1 showing location and values of heat flow measurements in survey D1. The strong reflections in the central part of both profiles mark the Messinian salt series, with basement ridges to the north, south, and west. (*b*) Numerical models of thermal refraction, profile SH3/81P1. The input model, based on the seismic sections in Figure 5*a*, is shown beneath the computed surface flux (continuous line) and observed data (errors marked at the 95% confidence level).

buried basement highs and to the east by a diapiric salt structure. The sharp horizon which occurs in the reflection record between 4.0 and 4.5 s can be correlated with a hiatus drilled at site 372 and marks the top of the Messinian salt series.

Linear temperature gradients were recorded throughout most of the survey, but owing to instrumental problems, no in situ conductivity values were recovered. Conductivity was therefore assigned from the needle probe values measured on core C1; these were remarkably uniform except for a very narrow band of high-conductivity material at 2.3 m (Figure A1). It is thought that the slight kink in the temperature gradients found at stations 1.4, 2.1, and 2.2 may be caused by this high-conductivity layer. Calculating the mean heat flow and uncertainty for the survey yields the values

$$Q = 92 \pm 10 \text{ mW m}^{-2} \quad (95\% \text{ confidence level})$$

for $N = 12$, $\sigma = 14$. The value of 102 mW m^{-2} measured through the uppermost 300 m of sediment at DSDP site 372A [*Erickson and Von Herzen*, 1978] lies within this range, suggesting that the surface fluxes are a reliable indicator of the total conductive flux and are not significantly biased by any recent environmental or water temperature changes.

Despite the thick sediment cover, the heat flow shows a marked spatial variability, with a maximum deviation of 25% from the mean at station 2.6 (117 mW m^{-2}). The most likely source of these variations is refraction of heat through the accumulations of high-conductivity salt and evaporite. To account for this effect, a two-dimensional numerical model was used to calculate theoretical heat flow profiles along the seismic sections in Figure 5. The model was based on a computer program developed by P. C. England [e.g., *England et al.*, 1980], which calculates the steady state temperatures in a body of variable thermal conductivity. The following boundary conditions applied: (1) surface temperature is constant, (2) uniform heat flux of the survey mean value across the lower boundary set at a depth 3–4 times greater than the deepest conductivity interface, and (3) no heat is allowed to flow through the sides of the model. The sections were divided into three conductivity regions: (1) Plio-Quaternary sediment, (2) salt and evaporite, and (3) basement and pre-Messinian sediments, with estimated conductivity contrasts of 1 : 4 : 2, respectively. Using interval velocities of 2, 4, and 5 km s^{-1} [*Finetti and Morelli*, 1973], the travel times to the upper surfaces of regions 2 and 3 were converted to the depth sections shown in Figure 5*b*.

While the details of the measured values deviate from the model predictions (Figure 5), the general trends are well matched, especially in the N-S line where the broad high in

the surface heat flow is clearly related to the thicker and shallower accumulations of salt. In considering these models the following points should be noted: (1) the conductivity structure is strongly three-dimensional, thus any two-dimensional model can give only an approximate solution, (2) the measured fluxes are projected onto the profiles from as much as 1 km distant, and (3) the chosen interpretation of the reflection records (and hence the conductivity structure) is not unique; in particular, the basement depth beneath the salt layer is poorly defined. Nonetheless, a number of alternative models were calculated by varying the conductivity contrasts and distributions, but any physically reasonable configurations produced only minor differences from the results shown in Figure 5.

The model demonstrates that the variability in the flux can be explained by the presence of high-conductivity salt and that since the measurements are distributed over at least one full wavelength of the expected anomalies, the spatial sampling of the data is sufficient to average the effects of the thermal refraction. Thus the calculated mean forms an unbiased estimate of the regional flux.

Before comparing the heat flow with theoretical cooling models, the blanketing effects of the rapidly deposited salt and sediment layers must be evaluated. A numerical analysis of the problems of sedimentation, accounting for compaction, pore water movement, and surface temperature changes has been developed to obtain accurate estimates of sediment correction factors [*Hutchison*, 1984]. The technique uses a one-dimensional finite difference scheme to model the temperature perturbations of the lithosphere under a variable sedimentation history. Advection rates of sediment particles, pore fluid, and basement are calculated separately, while sediment bulk conductivities and densities are obtained by combination of the sediment matrix and pore fluid values.

Different sediment porosity-depth relationships, based on data from the nearby DSDP sites, were obtained for the Balearic and Tyrrhenian basins (Table 3). Salt formations were treated separately and assigned appropriate physical properties. Two alternative types of boundary condition were used; in the first a constant flux was provided at the base of the model, in common with previous analytical methods, while the second assigned a constant temperature to the lower boundary, reflecting a cooling slab model of the lithosphere.

The relevant sedimentation rates and physical properties forming the model inputs for survey D1 were estimated from DSDP hole 372 and reflection profiles SH3/81P1 and IFPJ204 [*Hsu et al.*, 1978]. From the depth-converted sections in Figure 5 the Messinian and Plio-Quaternary sedimentation has been assigned as 750 m Messinian salt deposited between 6.6 and 5.2 Ma, followed by mudstone deposition at a constant rate of 120 m m.y.$^{-1}$ to the present. The amount of earlier sedimentation is unknown, principally because the strongly reflecting salt layers obscure later returns in the seismic records. Thus, to account for the sediment cover, two models have been considered: the first neglects any pre-Messinian sedimentation, while the second assigns the maximum pre-Messinian sedimentation rates ($\sim$100 m m.y.$^{-1}$) found at DSDP site 372 to the period from its formation at a

TABLE 3. Sedimentation Corrections: Model Input Parameters

	Density, kg m^{-3}	Specific Heat, J kg^{-1} K^{-1}	Conductivity, W m^{-1} K^{-1}
Water	1030.0	4186.0	0.670
Salt	2160.0	854.0	5.858
Basement	3330.0	1170.0	3.099
Sediment matrix	2700.0	900.0	2.500

Surface porosity P_0: survey D1 = 60%, surveys D2 and D3 = 65%; Sediment compaction constant a: survey D1 = 1200 m, surveys D2 and D3 = 2000 m. For the purposes of the model the sediment is assumed to have a porosity depth dependence of $P(z) = P_0 e^{-z/a}$, where P is the porosity and a is the compaction constant.

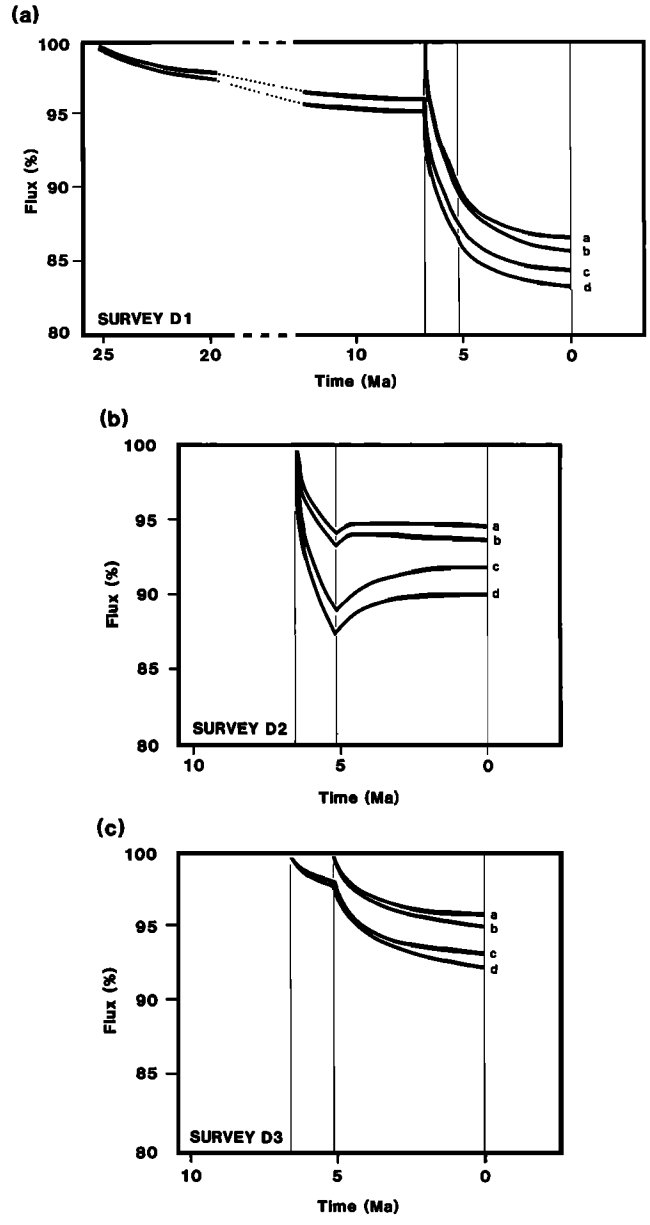

Fig. 6. Calculated alteration to the geothermal flux due to the deposition of sediment at sites D1, D2, and D3. (*a*) Messinian and Plio-Quaternary sedimentation as given in text, curve a, constant flux, and curve b, cooling plate boundary conditions; additional pre-Messinian sedimentation at 100 m m.y.$^{-1}$ since origin at maximum age of 25 Ma; curve c, constant flux model, and curve d, plate model. (*b*) Messinian deposition at 500 m m.y.$^{-1}$ followed by Plio-Quaternary sedimentation at 38 m m.y.$^{-1}$ curve a, constant flux, and curve b, cooling plate boundary conditions; Messinian deposition at 100 m m.y.$^{-1}$ and Plio-Quaternary sedimentation as above; curve c, constant flux, and curve d, plate boundary conditions. (*c*) Curves a and b, Plio-Quaternary deposition at 80 m m.y.$^{-1}$; curves c and d, Messinian sedimentation at a rate of 200 m m.y.$^{-1}$, calculated for constant flux and cooling plate boundary conditions, respectively.

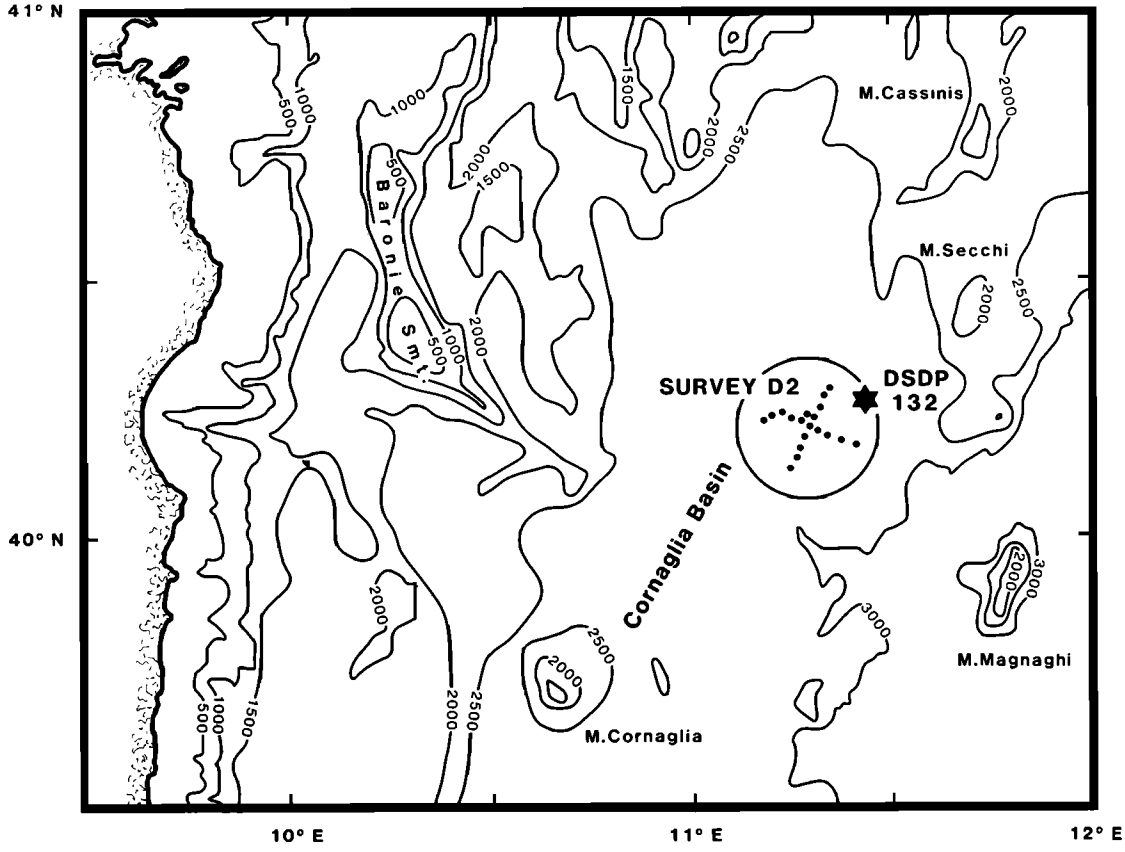

Fig. 7. Location of survey D2, Cornaglia basin (bathymetry in meters).

maximum age of 25 Ma to the Messinian at 6.7 Ma. The estimated alterations to the heat flow are shown in Figure 6*a*. These calculations show that the present heat flow is reduced to between 82 and 88% of that expected in the absence of sedimentation. This suggests that the measured value should be multiplied by a factor of 1.18 ± 0.04 to obtain the corrected geothermal heat flux, giving a value of

$$Q_c = 109 \pm 15 \text{ mW m}^{-2}$$

SURVEY D2

Eighteen heat flow measurements were taken in survey D2, located in the central Cornaglia basin, approximately 100 km east of Sardinia (Figure 7). At a water depth of 2870 m the basin has complete Plio-Quaternary sediment cover over the only substantial deposits of Messinian salt found in the Tyrrhenian, as shown in reflection profile SH3/81T1 (Figure 8*a*). At DSDP site 132, on the northeastern limit of the survey area, drilling penetrated 188 m of pelagic ooze before encountering solid gypsum rock of Messinian age [*Ryan et al.*, 1973]. To the northwest the area is bounded by continental material found in the Cassinis, Baronie, and Cornaglia seamounts, while southeast of the survey the basin trends toward the volcanic Magnaghi seamount and the oceanic abyssal plain. Seismic refraction results [*Nicholich*, 1981] suggest a crustal thickness of 10–15 km just north of this area, while interpretations of a refraction profile shot along line SH3/81T1 on the *Shackleton* cruise suggest a total crustal thickness of 9 km, with the upper 2–3 km formed from lower-velocity sediments and salt [*Duschenes*, 1983]. Subsediment seismic velocities in the southern part of line T1 are typical of oceanic crust, but the velocities in the northern section are lower and more representative of continental material. The crustal thickness does not vary significantly along the profile, suggesting that the basin is underlain by transitional oceanic/highly stretched continental crust.

The calculated heat flows are listed in Table 2, and their values and positions plotted in Appendix A, Figure A4. The recorded temperature gradients and calculated in situ conductivities are shown in Figure A5. The stations lying on the N-S line of the survey are shown on part of the reflection profile SH3/81T1 in Figure 8*a*. The data quality was generally good, with seven individual in situ conductivity determinations and well-defined linear temperature gradients. The correlation between conductivities from core C2 and the in situ values at the nearest heat flow station (6.3) is excellent (Figure 3).

The survey mean and uncertainty have been calculated as

$$Q = 134 \pm 8 \text{ mW m}^{-2} \quad (95\% \text{ confidence level})$$

for $N = 18$, $\sigma = 23$.

Following the method developed previously, a theoretical heat flow profile along T1 was computed in an attempt to explain the observed variability in the geothermal flux. *Ryan et al.* [1973] estimate that the thickness of the salt may be 1.0–1.5 km in the Cornaglia basin; so for the purposes of the thermal model, the lower boundary of the salt was placed at 1.5 km subbottom. J. P. Rehault (personal communication, 1983) has suggested that the thickness of the Messinian sequence may not exceed 500 m, but the perturbation in the surface flux is less sensitive to the total thickness than to the surface topography of the salt. The computed flux (Figure 8*b*)

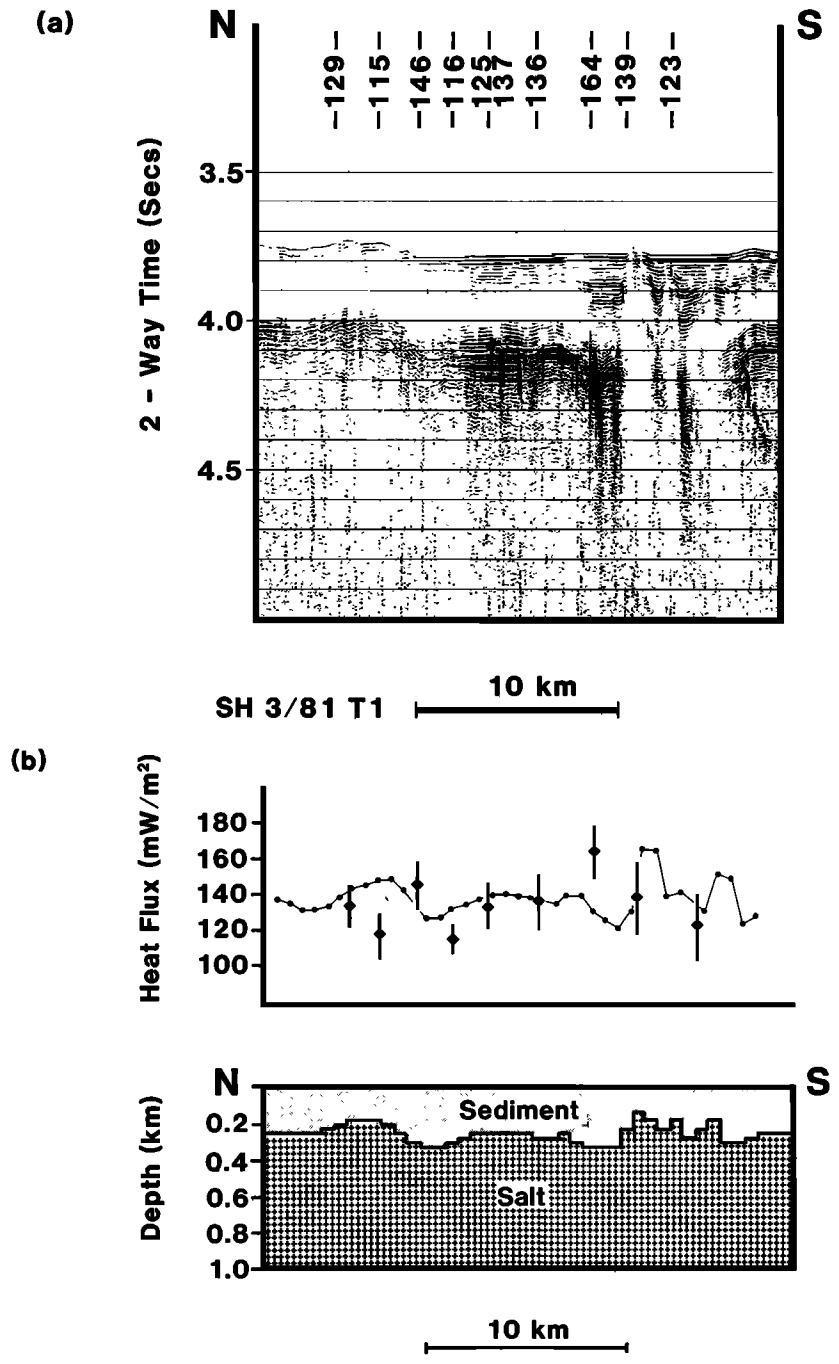

Fig. 8. (*a*) Part of reflection profile SH3/81T1, showing the positions and values of heat flow measurements on the N-S line of survey D2. Correlation with drilling at DSDP site 132 [*Ryan et al.*, 1973] shows that the prominent reflectors at 4 s mark the top of the Messinian evaporite sequence. Note the salt diapir toward the southern end of the profile. (*b*) Surface heat flux computed by a two-dimensional thermal refraction model from the crustal configuration shown in Figure 8*a*. Surficial sediments are assumed to be underlain by thick accumulations of salt with a conductivity contrast of 1 : 4.

shows significant lateral variations, and while the measured values do not agree particularly well in detail with the numerical model, the amplitude of the observed anomalies is consistent with the effects of thermal refraction. Once again, the influence of off-profile features might account for the deviations between the calculated and observed values, although the possibility of other processes, such as fluid circulation, cannot be discounted.

Sedimentation corrections have been calculated using the procedures outlined previously. Pre-Messinian sedimentation history is virtually unknown, but in view of the short time between basin formation and deposition of the salt, it seems unlikely that anything other than very high sedimentation rates would have affected the heat flux significantly. Thus the corrections have been calculated for Messinian and Plio-Quaternary deposition only, with sedimentation rates and physical properties from DSDP site 123 (summarized in Table 3). Post-Miocene sedimentation has continued at 38 m m.y.$^{-1}$, giving rise to approximately 200 m of sediment cover over the salt horizon. Since the thickness of the salt layer is unknown,

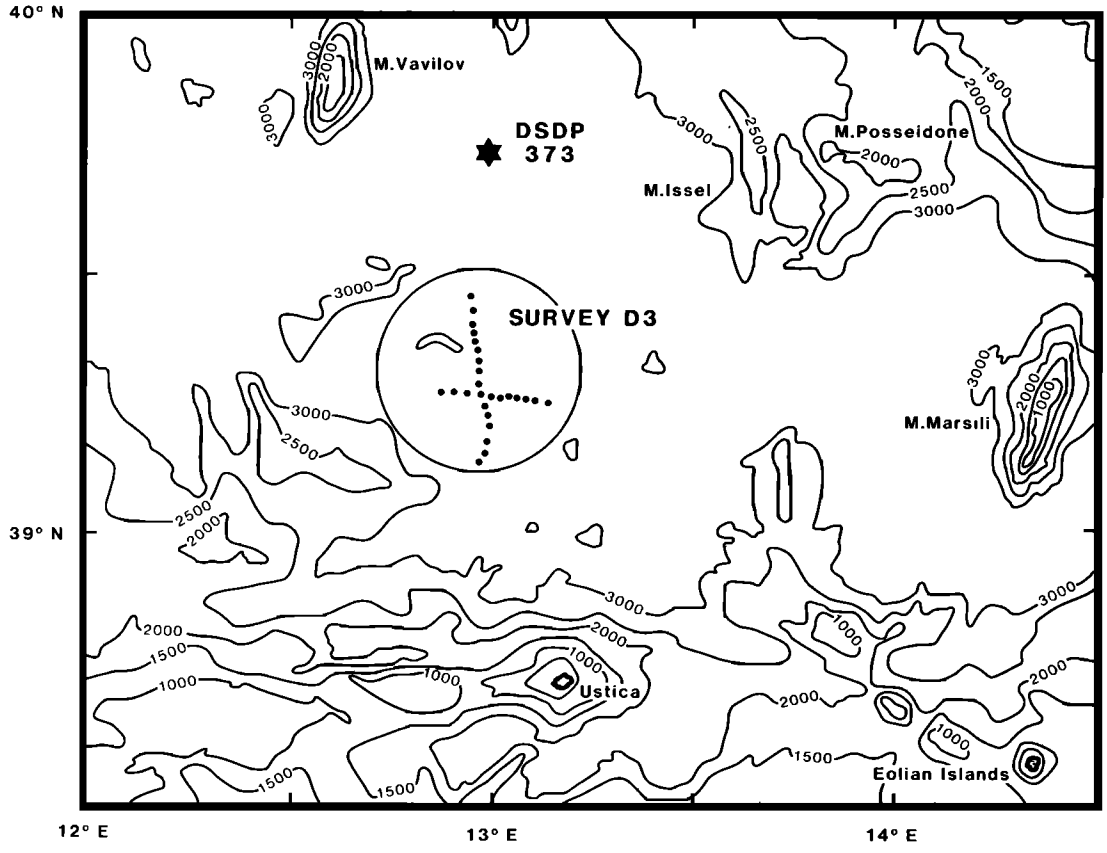

Fig. 9. Location of survey D3, southern Tyrrhenian Sea (bathymetry in meters).

two models have been evaluated, with Messinian deposition at 500 and 1000 m m.y.$^{-1}$, giving between 700 and 1400 m of salt. Figure 6*b* shows the resulting variations of flux through time. The Messinian deposition is the most important factor in determining the present heat flow, the light Plio-Quaternary sedimentation causing little subsequent alteration to the flux. The present value is seen to lie between 90 and 95% of the original, giving correction factors of 1.05–1.11. This yields a sedimentation-corrected flux of

$$Q_c = 145 \pm 13 \text{ mW m}^{-2}$$

SURVEY D3

Survey D3 lies approximately 180 km southeast of D2, in the southern Tyrrhenian abyssal plain (Figure 9). The area is ringed by volcanic seamounts and islands: to the northwest, Mount Vavilov; to the east, Mount Marsili; and to the south and southeast, Ustica and the Eolian Islands. Figure 10*a* shows part of the N-S reflection profile SH3/81T2, along which are located 17 of the 26 heat flow stations in the survey. The area is marked by a topographic high of about 100 m relief, which extends from the center of the survey to the northwest. Sediment cover occurs over the entire area with accumulations of up to 500 m in the northern part of the survey. The nature of the underlying material is uncertain; *Fabbri and Curzi* [1979] claim that in excess of 200 m evaporites were deposited in the region during the Messinian, while *Malinverno et al.* [1981] suggest that the area was subject to subaerial clastic sedimentation at that time. The nature of the subsediment reflections seen in line T2 is quite different in character from those observed from the salt horizons in surveys D1 and D2, their generally unclear and scattered signature being more typical of volcanic basement than of salt returns. The crust itself is almost certainly oceanic; 3–7 Ma oceanic basalts were found at DSDP site 373, 50 km north of the survey, and seismic refraction results from the same area [*Nicholich*, 1981] suggest a crustal thickness of 6–7 km. This is supported by the results from a refraction profile shot along line SH3/81T2, which shows an average crustal section of between 6 and 7 km depth with about 500 m of surficial sediments [*Duschenes*, 1983].

The calculated heat fluxes are given in Table 2 and plotted in Appendix A, Figure A6. Measured gradients and calculated in situ conductivities are shown in Figure A7. This was the best data set from the three surveys, with all stations recording at least five independent temperature depth points and station groups 7 and 8 with nine points over a 4-m span. Despite the high and variable heat flows, the temperature profiles were generally linear. Fourteen stations have in situ conductivity profiles measured with the Cambridge probe, with a further five from the WHOI instrument. Conductivities from the WHOI probe show a greater variability than either the Cambridge in situ or the core C3 needle probe values, but the mean values fall within experimental error bounds. Once again, the correlation between Cambridge in situ and needle probe values was particularly good. A slight increase in conductivity from south to north across the survey area can be detected from the in situ data of station groups 7 and 8. Calculating the survey mean heat flow and its uncertainty gives

$$Q = 151 \pm 10 \text{ mW m}^{-2} \quad (95\% \text{ confidence level})$$

for $N = 26$, $\sigma = 25$.

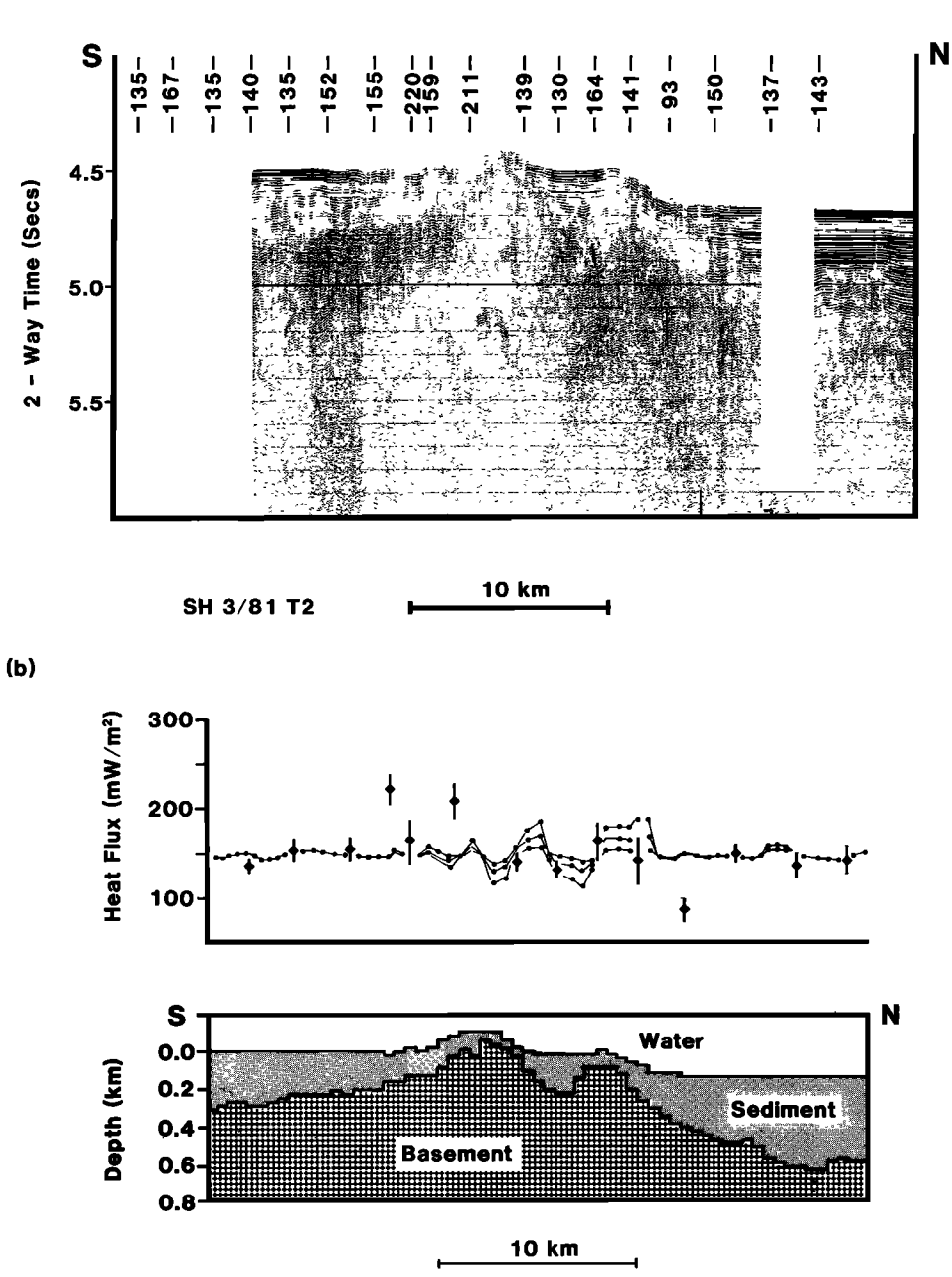

Fig. 10. (*a*) Reflection line SH3/81T2 (part) with the measured heat fluxes projected onto the profile. Note the higher values correlated with the topographic highs and the unusually low value of 93 mW m^{-2} at the foot of the slight scarp bounding the central abyssal plain. The value of 140 mW m^{-2} at the southern edge of the reflection profile is from *Erickson et al.* [1976]. (*b*) Surface heat flux computed from a two-dimensional model of the crustal configuration deduced from line SH3/81T2, with basement/sediment conductivity contrasts of 2 : 1, 4 : 1, and 8 : 1. The measured heat flows exhibit variations which are several times greater than those predicted by the numerical model, showing that thermal refraction cannot fully explain the heat flow trends in this area.

The most striking feature in the observed heat flow is the occurrence of unusually high and low values (e.g., stations 7.7 and 8.4 in Table 2 and Figure 10). Figure 10*b* shows the surface flux calculated from a two-dimensional thermal model along line T2. Since the nature of the underlying material (or its conductivity structure) is not known, the two-region model has been run for conductivity contrasts of 1 : 2, 1 : 4, and 1 : 8. The first of these ($K = 1:2$) is the most likely, reflecting the conductivity structure of sediment and volcanic basement. The latter two represent the case of sediment underlain by thick salt deposits. The results shown in Figure 10 clearly demonstrate that the scatter in this area cannot be fully explained by thermal refraction, since the observed amplitudes of the anomalies are several times greater than those calculated, even from models with unreasonably high-conductivity contrasts (i.e., 1 : 8). Similar results were obtained from models with alternative structural interpretations of line T2. Indeed, thermal refraction could only explain the observed values if extreme salt geometries were encountered at or near surface. Such structures cannot be resolved in the available seismic data.

Instead, the heat flow variations may be the result of hydrothermal circulation in young, porous basement beneath the

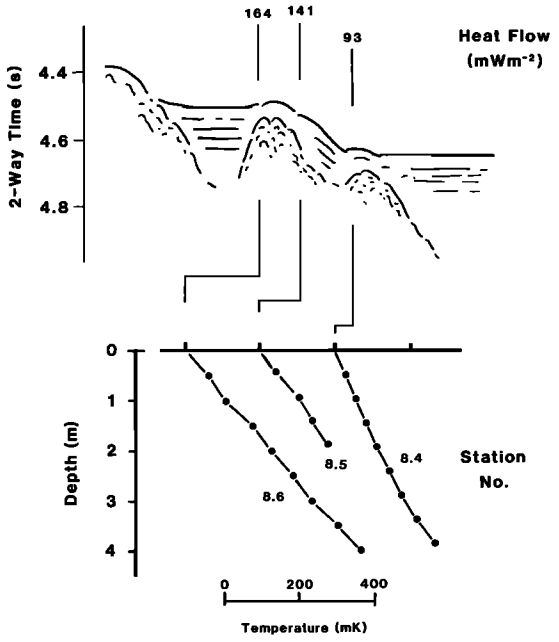

Fig. 11. Temperature profiles at stations 8.4, 8.5, and 8.6 over the northern scarp, shown in Figure 10. The correlation of heat flow with topography and the systematic curvature in temperature gradient at station 8.4 are typical of hydrothermal systems.

impermeable sediment cover. While the data set is not large enough to test this quantitatively, some qualitative observations can be made. First, the amplitude and wavelength of the anomalies are within the ranges found in other hydrothermal systems; e.g., although the crustal ages are significantly younger, *Green et al.* [1981] find topography-related heat flow variations in excess of 50% of the mean values over distances of about 5 km in the Galapagos hydrothermal field. Second, although the largest anomalies occur near the center of the profile, the most striking evidence of hydrothermal alteration of the heat flux is from stations 8.4, 8.5, and 8.6 (Figure 11 and Table 2) across a small scarp marking the southern edge of the central Tyrrhenian abyssal plain. Stations to the north and south of the feature show remarkably uniform values (140 mW m^{-2}, $\sigma = 6$ for stations 8.1, 8.2, 8.3, 8.7, and 8.8), but the flux at station 8.4, at the base of the scarp, is anomalously low (93 mW m^{-2}), while 8.6, on top of the slope, shows an unusually high heat flow (164 mW m^{-2}). Station 8.5, on the scarp face, gives a heat flux which is close to average for the area (141 mW m^{-2}). The sediment temperatures at station 8.4 show the only systematically curved gradient in the entire survey (Figures 11 and A7) and, although the in situ conductivity appears to decrease with depth, the variation is not sufficient to account for the observed curvature. The concave upward profile would be consistent with a downward fluid flow through the thin sediments at this station [e.g., *Becker and Von Herzen*, 1983]. The topography-related heat flux and the nonequilibrium flow at station 8.4 suggest that active fluid circulation is taking place in the underlying basement. The occurrence of higher heat flux over topographic highs with low values near the base of scarp slopes has also been found by *Williams et al.* [1974] in the Galapagos area and by *Lister* [1972], *Davis and Lister* [1977], and *Davis et al.* [1980] over the Juan de Fuca spreading center and is attributed to venting of hydrothermal fluids concentrated by surface fault systems and varying sediment thickness.

An alternative explanation of the effects shown in Figure 11 as the result of slumping downslope from the topographic high cannot be entirely ruled out. However, the observed variations and curvatures in gradient would require very recent sediment movement, and the probability of observation is very low [see *Noel*, 1984]. Also, in a slump environment the sediment conductivity could be expected to be irregular with higher values on the crest and low values in the slump material; the data in Table 2 and Figure A7 show that this does not occur.

Although the heat flow shows large variations in area D3, the anomalies are localized. Also, in the well-sedimented areas the values are closely grouped in the range of 135–165 mW m^{-2}. These facts suggest that any hydrothermal effects are of short wavelength (up to about 5 km), so that our survey extending over 40 km with 1–2 km station spacing should give an unbiased estimate of the regional conductive heat loss.

Area mean sedimentation corrections have been calculated for D3 using deposition rate and physical property data from hole 373, with the parameters listed in Table 3. Two deposition histories were considered: (1) post-Miocene sedimentation at a rate of 80 m m.y.$^{-1}$ only and (2) preceded by deposition of 200 m of salt during the Messinian. Both have been calculated for constant flux and cooling plate models with the results shown in Figure 6*c*. The present flux lies between 92 and 96% of the true value, giving a corrected heat flow of

$$Q_c = 161 \pm 14 \text{ mW m}^{-2}$$

It remains possible that a significant part of the total heat flow is removed by fluid circulation, so this estimate of the corrected conductive flux will form a minimum estimate of the true basal heat flow.

Discussion

Heat Flow, Age, and Crustal Structure

In Figure 12 the corrected heat fluxes from surveys D1, D2 and D3 have been plotted against (age)$^{-1/2}$, with the age ranges for the basins assigned from the earlier discussion on the evolution of the western Mediterranean. Also shown are the theoretical cooling curves for simple stretching models with $\beta = 4$, 6, and 10 and for the oceanic plate model ($\beta = \infty$). The values increase from survey D1 to D3, reflecting a trend toward higher heat flux from west to east through the Balearic and Tyrrhenian basins. Within the accuracy of the data and

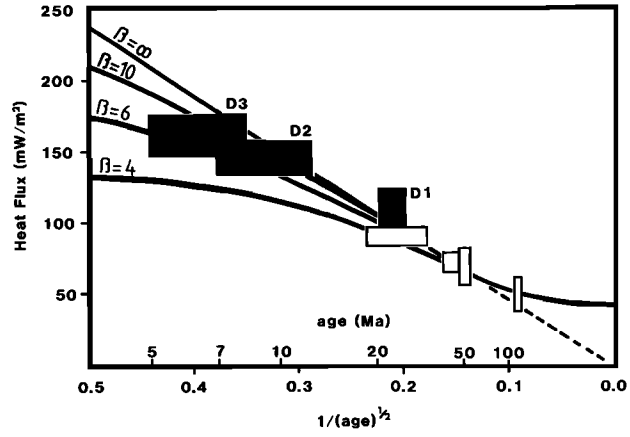

Fig. 12. Corrected heat fluxes from surveys D1, D2, and D3 plotted against $t^{-1/2}$ and compared with theoretical cooling curves from plate and simple stretching models. Reliable data from other marginal basins [*Sclater et al.*, 1980] are also shown.

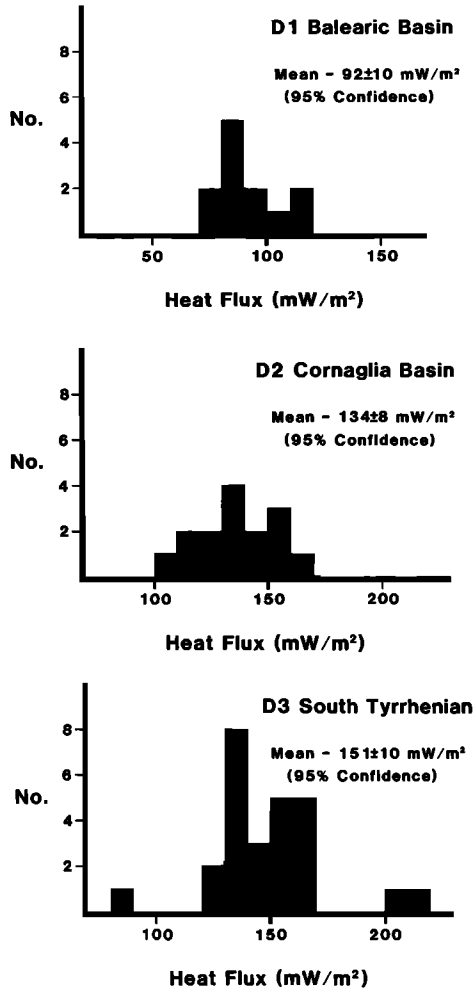

Fig. 13. Histograms showing the distribution of heat fluxes at the three survey sites; note the unusually high and low values in D3.

the uncertainty of the parameters used in calculating the theoretical cooling curves, the measured fluxes agree closely with those predicted by the plate model and high value ($\beta > 6$) stretching models. This result is consistent with the available data on the crustal structure in the survey areas which suggests that D1 and D2 are underlain by thinned continental or oceanic material, while D3 is almost certainly oceanic. Note that inclusion of an additional convective heat loss to account for fluid circulation on the third survey would shift the D3 data points closer to the expected plate model values.

Some care must be taken in interpreting stretching models with large values of β: while the total extension and the averaged heat flow predicted remain valid, the brittle continental crust does not become "infinitely thin" as extension is continued. Rather, in these transitional zones it is more likely that large blocks of continental material will become separated and intruded by "oceanic" basalts. Conventional estimation of β from the crustal thinning becomes impossible, since detailed measurement of the crustal structure will only reveal areas of oceanic crust interspersed with discrete continental fragments [e.g., *Duschenes*, 1983; *Moussat*, 1983]. For example, in area D2 the Cornaglia basin is at least partly oceanic [*Duschenes*, 1983] but is surrounded by seamounts of continental material. In the same way, it is unlikely that well-developed ridge spreading systems will be found in such areas, and consequently, clearly defined seafloor spreading magnetic anomalies cannot be expected. While the oceanic plate and high-β stretching models cannot be resolved by thermal measurements, the models do provide an adequate account of the overall thermal balance of basin formation.

The values of other reliable marginal basin heat flow data [from *Sclater et al.*, 1980] have also been plotted in Figure 12. The overall agreement of the observed data compared with the plate model is good. Within the experimental errors, no significant difference exists between the heat loss as a function of age from the major oceans (characterized by the plate model) and from marginal and back arc basins. Conversely, the fit shows that heat flow can be used as an indicator of age for marginal basins which have experienced large amounts of extension and spreading.

Heat Flow Variability

The variability in the measured heat flux within each survey is large; Figure 13 shows the distribution of the measured values from the three survey areas. Numerical modeling of heat flow in areas D1 and D2 suggests that this can be explained by thermal refraction through highly conductive salt accumulations. However, the amplitude of the heat flow anomalies in area D3 remains too large to be ascribed entirely to steady state thermal refraction; other processes must occur to give the high variability observed, the most likely being hydrothermal circulation in the young and fractured oceanic basement. The higher heat flow over the central topographic high (station 8.6) with the anomalously low value at the base of the slight scarp (station 8.4) is similar to the trends observed by *Green et al.* [1981] in the Galapagos hydrothermal field. Additional evidence of hydrothermal activity in the area comes from the basalts recovered at site 373, which show considerable geochemical alteration due to the interaction with seawater. Also, other heat flow measurements in the Tyrrhenian Sea [*Erickson et al.*, 1976; B. Della-Vedova, personal communication, 1982; J. P. Foucher, personal communication, 1981] show that the values found near large volcanic seamounts are often anomalously low, probably as a result of the removal of heat by hydrothermal fluids venting through the exposed basement.

The data presented in this paper are the first to investigate quantitatively the detailed heat flow variability within the Balearic and Tyrrhenian basins and serve to emphasize the need for extensive multipenetration surveys. Only when a large number of closely spaced measurements are made can the area mean flux and uncertainty be properly assigned. On the basis of this work it is evident that any individual measurement might vary by as much as 40–50% from the regional mean. This offers some explanation of the largely confusing picture which has evolved from preexisting data from the area, almost all of which is from single values, often affected by the local environment of the measurement.

Other Data: Tyrrhenian Sea Heat Flow and Basin Formation

Although few western Mediterranean heat flow values existed before 1977 [*Erickson et al.*, 1976], large numbers of new measurements have been made during the last 5 years. While the Balearic remains largely unexplored, a further 177 Tyrrhenian Sea heat flow stations are known in addition to the *Shackleton* 3/81 data. From these stations we are aware of 125 documented values.

Figure 14 shows a compilation of the available Tyrrhenian Sea heat flow data. The values have been grouped into areas enclosing approximately 10 measurements, allowing regional

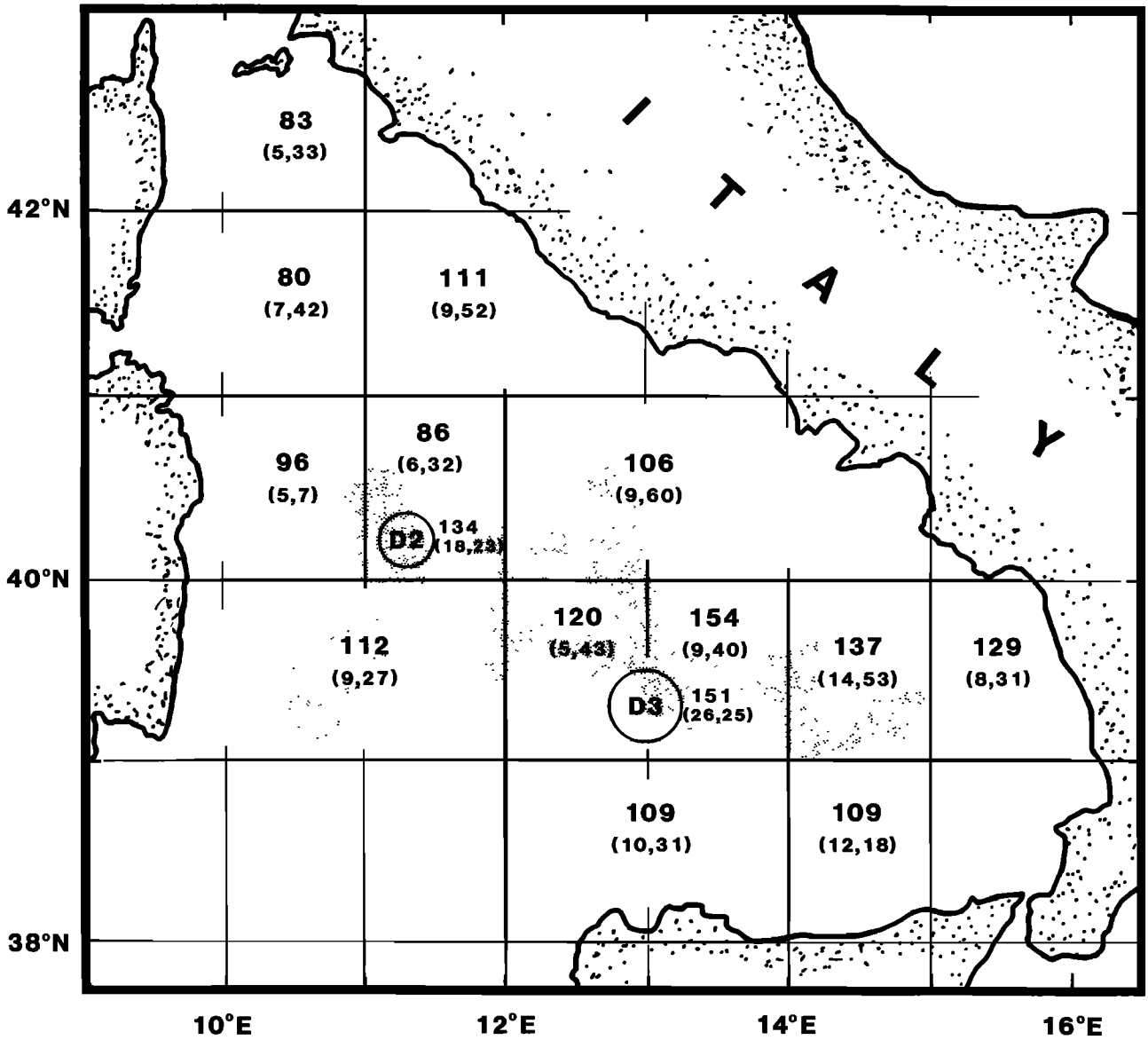

Fig. 14. Compilation of reliable Tyrrhenian Sea heat flow data, showing area average heat flux in milliwatts per square meter. The figures in parentheses are the number of data points used in forming the averages and the standard deviations, respectively. Results from surveys D2 and D3 are shown separately. The shaded regions indicate the major basinal and abyssal plain areas.

averages to be estimated. Anomalously high or low values associated with nearby seamounts or basement outcrops have been excluded from the data set. Nonetheless, the standard deviations from the means (Figure 14) show that the variability within each area remains large. No sedimentation corrections have been applied; thus the values will typically underestimate the true flux by 5–10%. A number of trends in the regional heat flow can be observed. In the northern Tyrrhenian and around the basin margins the flux is low for such a young basin, probably as a result of the moderately small amounts of extension and spreading experienced by these areas. In contrast, the major basinal and abyssal plain areas (shaded in Figure 14) show higher values, with the trend of increased flux to the southeast found between surveys D2 and D3 supported by the larger data set.

The trend of higher heat flow in the southeast is consistent with the estimates of basin age discussed previously and favors the model of basin formation behind a southeastwardly migrating trench-arc system in which the youngest areas would be found closest to the arc. If the $(\text{age})^{-1/2}$ plate cooling model is assumed correct for the oceanic areas, then the heat flux in the western (Cornaglia) and southeastern basins reflects ages of about 12 and 8 Ma, respectively. Figure 15 outlines a model describing the way in which these age differences might explain the observed variations in Messinian salt distribution and present basin depths. While the absolute depths of marginal basins appear to be greater than those of the major oceans, the increase of depth with age is similar [*Louden*, 1980]. Assuming that the subsidence is given by 350 m $(\text{age})^{1/2}$ [*Sclater et al.*, 1980], the relative depths of the western and southeastern Tyrrhenian basins have been estimated through time. At the start of the Messinian the Tyrrhenian would have been about 400 m deeper to the west. In a simple dessication model [e.g., *Hsu et al.*, 1973], salt will deposit in the deepest parts of the basin first; because of the different densities of basalt, salt, and water, a total thickness of about 700 m of salt

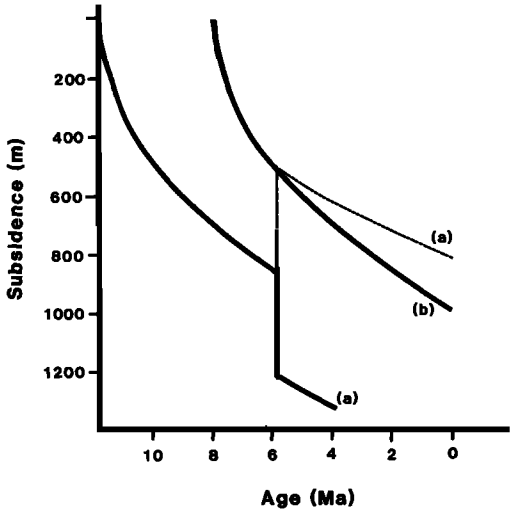

Fig. 15. Speculative model to illustrate the subsidence of (curve a) the western and (curve b) southeastern Tyrrhenian basins. Ages of formation have been estimated from the shaded area average heat flows given in Figure 14. The southereastern basin is about 400 m shallower at the start of the Messinian. Filling of the western basin to the same level as the southeastern area required a total thickness of about 700 m of salt to maintain isostatic equilibrium, explaining the thick section of Messinian salt found in the Cornaglia basin. Post-Miocene differential subsidence gives the present basin configuration, with the younger southeast basin at a slightly greater depth. The solid curves trace the subsidence of the basement, while the dashed line shows the upper surface of the salt layer.

is required to adjust the seafloor depth in the western basin to be the same as the southeast and yet maintain local isostasy at that time. This value is within the range of 500–1500 m of salt estimated for the Cornaglia basin. Post-Miocene subsidence gives the present depth of the younger basin to be about 200 m greater; in view of the simplicity of the model and its neglect of sediment loading and flexural effects, this value agrees well with the difference of about 500 m observed between the present abyssal plain and the Cornaglia basin. A younger southeastern Tyrrhenian (as suggested by the site 373 basalts) would account for greater differences in the present bathymetry. These results are in broad agreement with the conclusions of *Fabbri and Curzi* [1979], who favor a deep western basin at the time of the Messinian and Plio-Quaternary subsidence in the southeast, based on evidence from seismic reflection profiles.

The question of Messinian paleogeography of the Tyrrhenian is also discussed by *Malinverno* [1981] and *Malinverno et al.* [1981]. By comparing mostly pre-1977 heat flow measurements and corrected basement depths with the predictions of the oceanic plate and stretching models, age estimates of 10–14 Ma were obtained for the basin. On the basis of these estimates, *Malinverno et al.* [1981] conclude that the Messinian morphology of the Tyrrhenian need not have been significantly different from that observed today and that detailed relationships between topography and drainage patterns were responsible for the lack of major Messinian deposits in the southeastern basin. Their analysis is incomplete on two counts; first, the heat flow measurements used are inadequate to allow realistic estimate of the regional heat flux because they are contaminated by anomalously low values measured near major basement outcrops, and second, their use of normal ocean floor bathymetry as an indicator of crustal age is invalid since it has been shown [e.g., *Louden*, 1980] that the depths of marginal basins are consistently 500–1000 m deeper than those predicted by the best fit plate models.

In contrast, the data presented here offer a self-consistent model of basin development and timing, accounting for heat flow, crustal structure, ages, and Messinian evaporite distributions.

Summary

1. Heat flow increases from west to east through the Balearic and Tyrrhenian basins.
2. Heat flow versus age follows the same curves as those predicted by plate cooling for the major ocean basins; the only acceptable alternative models are based on thinned continental lithosphere with high stretching factors ($\beta > 6$).
3. Large local scatter in the heat flow can be attributed to thermal refraction through highly conductive salt structures in areas D1 and D2, but alternative processes (possibly including hydrothermal circulation) are required to account for the amplitude of the variability in survey D3.
4. Consideration of heat flow, age estimates, and distribution of Messinian salt and evaporites favors models of formation of the Tyrrhenian Sea behind a southeastwardly migrating trench-arc system, with the older areas of the basin now found in the west.

Acknowledgments. Funding for ship time and the Cambridge heat flow project was provided by the United Kingdom Natural Environmental Research Council (NERC) awards GR3/3933 and ER3/4696. The groups from Woods Hole and the Massachusetts Institute of Technology were backed under U.S. National Science Foundation grants OCE-8025181 and OCE-8024287. Iain Hutchison acknowledges the support throughout this work of a Shell International Oil Company research studentship. Also, for their extensive and greatly valued assistance both in preparation for the cruise and at sea we wish to thank the following: from the Bullard Laboratories, Cambridge, Tim Owen, Melvin Mason, Mike MacCormack, and Angus Goudie; from the NERC Research Vessel Base, Stan Smith and Ivor Chivers; and from Woods Hole, George Pelletier, Dave Goldstein, and Jim Broda. University of Cambridge, Department of Earth Sciences contribution 429. Contribution 5745 from the Woods Hole Oceanographic Institution.

References

Alvarez, W., T. Cocozza, and F. C. Wezzel, Fragmentation of the Alpine orogenic belt by microplate dispersal, *Nature, 248*, 309–314, 1974.

Anderson, R. N., Update of heat flow in the east and southeast Asian seas, in *The Tectonic and Geologic Evolution of Southeast Asian Seas and Islands, Geophys Monogr. Ser.*, vol. 23, edited by D. E. Hayes, pp. 319–326, AGU, Washington, D. C., 1980.

Auzende, J. M., J. M. Bonnin, and J. L. Olivet, The origin of the western Mediterranean basins, *J. Geol. Soc. London, 129*, 607–620, 1973.

Barberi, F., P. Gasparini, F. Innocenti, and L. Villari, Volcanism of the southern Tyrrhenian sea and its geodynamic implications, *J. Geophys. Res., 78*, 5221–5232, 1973.

Barberi, F., H. Bizouard, G. Capaldi, G. Ferrara, P. Gasparini, F. Innocenti, J. L. Juron., B. Lambert, M. Treuil, and C. Allegre, Age and nature of basalts from the Tyrrhenian abyssal plain, *Initial Rep. Deep Sea Drill. Proj., 42*(1), 509–514, 1978.

Becker, K., and R. P. Von Herzen, Heat transfer through the sediments of the Mounds hydrothermal area, Galapagos spreading center at 86°W, *J. Geophys. Res., 88*, 995–1008, 1983.

Biji-Duval, B., J. Letouzey, and L. Montadert, Structure and evolution of the Mediterranean basins, *Initial Rep. Deep Sea Drill. Proj., 42*(1), 951–984, 1978.

Boccaletti, M., and G. Guazzone, Remnant arcs and marginal basins in the Cainozoic development of the Mediterranean, *Nature, 252*, 18–21, 1974.

Bullard, E. C., The flow of heat through the floor of the Atlantic Ocean, *Proc. R. Soc. London Ser. A, 222*, 408–429, 1954.

Burrus, J., Contribution to a geodynamic synthesis of the Provencal basin (NW Mediterranean), *Mar. Geol., 55*, 247–269, 1984.

Davis, E. E., and C. R. B. Lister, Heat flow measured over the Juan da Fuca ridge: Evidence for widespread hydrothermal circulation in a highly heat transportive crust, *J. Geophys. Res., 82*, 4845–4860, 1977.

Davis, E. E., C. R. B. Lister, U. S. Wade, and R. D. Hyndman, Detailed heat flow measurements over the Juan de Fuca ridge system, *J. Geophys. Res., 85*, 299–310, 1980.

Duschenes, J. D., Aspects of ocean bottom seismology, Ph.D. thesis, Univ. of Cambridge, Cambridge, 1983.

England, P. C., E. R. Oxburgh, and S. W. Richardson, Heat refraction and heat production in and around granite plutons in north-east England, *Geophys. J. R. Astron. Soc., 62*, 431–455, 1980.

Erickson, A. J., and R. P. Von Herzen, Down-hole temperature Measurements, Deep Sea Drilling Project, leg 42A, *Initial Rep. Deep Sea Drill. Proj., 42*(1), 857–871, 1978.

Erickson, A. J., G. Simmons, and W. B. F. Ryan, Review of heat flow data from the Mediterranean and Aegean Seas, in *XXV CIESM Congress, Structural History of the Mediterranean Sea Basins*, edited by B. Biju-Duval and L. Montadert, pp. 263–279, Editions Technip, Split, Yugoslavia, 1976.

Fabbri, A., and P. Curzi, The Messinian of the Tyrrhenian seismic evidence and dynamic implications, *G. Geol., 43*(1), 215–248, 1979.

Fahlquist, D. A., and J. B. Hersey, Seismic refraction measurements in the western Mediterranean Sea, *Bull. Inst. Oceanogr., 67*(1386), 52, 1969.

Finetti, I., and C. Morelli, Geophysical exploration of the Mediterranean Sea, *Boll. Geofis. Teor. Appl., 15*, 263–341, 1973.

Galdeano, A., and J. I. Rossignol, Assemblage a altitude constante des carts d'anomalies magnetiques couvrant l'ensemble du bassin occidental de la Mediterranee, *Bull. Soc. Geol. Fr., 19*, 461–468, 1977.

Goldberg, D., R. P. Von Herzen, and J. G. Sclater, Thermal conductivity measurement of fused silica glass, *W.H.O.I. Tech. Rep. WHOI-80-34*, Woods Hole Oceanogr. Inst., Woods Hole, Mass., 1980.

Green, K. E., R. P. Von Herzen, and D. L. Williams, The Galapagos spreading center at 86°W: A detailed geothermal field study, *J. Geophys. Res., 86*, 979–986, 1981.

Hinz, K., Results of seismic refraction investigations (Project Anna) in the western Mediterranean Sea, south and north of the island of Mallorca. *Bull. Cent. Rech. Pau, 6*(2), 405–426, 1972.

Hsu, K. J., Tectonic evolution of the Mediterranean basins, in *The Ocean Basin and Margins*, vol. 4A, edited by A. E. M. Nairn, W. H. Kanes, and F. G. Stehli, pp. 29–75, Plenum, New York, 1978.

Hsu, K. J., M. B. Cita, and W. B. F. Ryan, The origin of the Mediterranean evaporites, *Initial Rep. Deep Sea Drill. Proj., 13*(2), 1203–1231, 1973.

Hsu, K. J., et. al. (Eds.), Site 372: Menorca Rise, *Initial Rep. Deep Sea Drill. Proj., 42*(1), 59–150, 1978.

Hutchison, I., Heat flow studies in the Gulf of Oman and western Mediterranean, Ph.D thesis, Univ. of Cambridge, Cambridge, 1983.

Hutchison, I., The effects of sedimentation and compaction on oceanic heat flow, *Geophys. J. R. Astron. Soc.*, in press, 1984.

Hyndman, R. K., E. E. Davis, and J. A. Wright, The measurement of marine geothermal heat flow by a multi-penetration probe with digital acoustic telemetry and in-situ thermal conductivity, *Mar. Geophys. Res., 4*, 181–205, 1979.

Karig, D. E., Ridges and basins of the Tonga-Kermadec island arc system, *J. Geophys. Res., 75*, 239–254, 1970.

Lister, C. R. B., On the thermal balance of a mid-ocean ridge, *Geophys. J. R. Astron. Soc., 26*, 515–535, 1972.

Lister, C. R. B., The pulse probe method of conductivity measurement, *Geophys. J. R. Astron. Soc., 57*, 451–461, 1979.

Lort, J. M., Geophysics of the Mediterranean Sea basins, in *The Ocean Basins and Margins*, vol. 4A, edited by A. E. M. Nairn, W. H. Kanes, and F. G. Stehli, pp. 151–214, New York, 1978.

Louden, K. E., The crustal and lithospheric thickness of the Philippine Sea as compared to the Pacific, *Earth Planet. Sci. Lett., 50*, 275–288, 1980.

Malinverno, A., Quantitative estimates of age and Messinian paleobathmetry of the Tyrrhenian Sea after seismic reflection, heat flow and geophysical models, *Boll. Geophys. Teor. Appl., 23*(90–91), 159–171, 1981.

Malinverno, A., M. Cafiero, W. B. F. Ryan, and M. B. Cita, Distribution of Messinian erosional surfaces beneath the Tyrrhenian Sea: Geodynamic Implications, *Oceanol. Acta, 4*, 489–495, 1981.

McKenzie, D. P., Some remarks on the development of sedimentary basins, *Earth Planet. Sci. Lett., 40*, 25–32, 1978*a*.

McKenzie, D. P., Active rectonics of the Alpine-Himalayan belt: The Aegean Sea and surrounding regions, *Geophys. J. R. Astron. Soc., 55*, 217–254, 1978*b*.

Montadert, L., J. Letouzey, and A. Mauffret, Messinian event: Seismic evidence, *Initial Rep. Deep Sea Drill. Proj., 42*(1), 1037–1050, 1978.

Montigny, R., J. B. Edel, and R. Thuizat, Oligo-Miocene rotation of Sardinia; K-Ar ages and paleomagnetic data of Tertiary volcanics, *Earth Planet. Sci. Lett., 54*, 261–271, 1981.

Moussat, E., Évolution de la mer Tyrrhenienne centrale et orientale et de ses marges septontrionales en relation avec la neotectonique dans l'arc Calabrais, doctoral thesis, L'Univ. Pierre et Marie Curie, Paris, 1983.

Nicholich, R., Il Profilo La line-Pescara E Le Registrazioni Mediante OBS Nel Mar Tirreno, paper presented at 1st Congres del Grappo Nazionale Geofisis Terra, Rome, Nov. 3–5, 1981.

Noel, M., Origins and significance of non-linear temperature profiles in deep sea sediments, *Geophys. J. R. Astron. Soc., 76*, 673–690, 1984.

Parsons, B., and J. G. Sclater, An analysis of the variation of ocean floor bathymetry and heat flow with age, *J. Geophys. Res., 82*, 803–827, 1977.

Ratcliffe, A. E., The thermal conductivities of ocean sediments, *J. Geophys. Res., 65*, 1535–1541, 1960.

Ritsema, A. R., On the origin of the western Mediterranean Sea basins, *Tectonophysics, 10*, 609–623, 1970.

Ryan, W. B. F., and M. B. Cita, The nature and distribution of Messinian erosional surfaces-indicators of a several kilometre deep Mediterranean in the Miocene, *Mar. Geol., 27*, 193–230, 1978.

Ryan, W. B. F., et al. (Eds.), Tyrrhenian Rise, site 132, *Initial Rep. Deep Sea Drill. Proj., 42*(1), 403–466, 1973.

Sclater, J. G., C. Jaupart, and D. Galson, The heat flow through oceanic and continental crust and the heat loss of the earth, *Rev. Geophys. Space. Phys., 18*, 269–311, 1980.

Von Herzen, R. P., and A. E. Maxwell, The measurement of thermal conductivity of deep sea sediments by a needle probe method, *J. Geophys. Res., 64*, 1557–1564, 1959.

Von Herzen, R. P., R. S. Detrick, S. T. Crough, D. Epp, and U. Fehn, Thermal origin of the Hawaiian swell: Heat flow evidence and thermal models, *J. Geophys. Res., 87*, 6711–6724, 1982.

Williams, D. C., R. P. Von Herzen, J. G. Sclater, and R. N. Anderson, The Galapagos spreading centre, lithospheric cooling and hydrothermal circulation, *Geophys. J. R. Astron. Soc., 38*, 587–608, 1974.

I. Hutchison, B. P. Exploration, Britannic House, Moor Lane, London, England EC2Y 9BU.

J. Jemsek, Department of Earth, Atmospheric and Planetary Sciences, Massachusetts Institute of Technology, Cambridge, MA 02139.

K. E. Louden, Department of Oceanography, Dalhousie University, Halifax, Nova Scotia, Canada B3H 4J1.

J. G. Sclater, Institute for Geophysics, University of Texas at Austin, Austin, TX 78712.

R. P. Von Herzen, Woods Hole Oceanographic Institution, Woods Hole, MA 02543.

(Received November 29, 1983;
revised August 13, 1984;
accepted August 24, 1984.)